Human-initiated autocyclic delta failures

Renaldo Gastineau, Stéphanie Girardclos, Katrina Kremer, Flavio S Anselmetti

SEDIMENTOLOGY the journal of the International Association of Sedimentologists IAS

Sedimentology (2024) doi: 10.1111/sed.13226

Human-initiated autocyclic delta failures

RENALDO GASTINEAU*,† , STÉPHANIE GIRARDCLOS‡ , KATRINA KREMER* and FLAVIO S. ANSELMETTI*

*Institute of Geological Sciences and Oeschger Centre for Climate Change Research, University of Bern, Baltzerstr. 1+3, Bern 3012, Switzerland (E-mail: renaldo.gastineau@univ-savoie.fr)

†EDYTEM, Université Savoie Mont-Blanc, CNRS, 5 bd de la mer Caspienne, Le Bourget du Lac 73376, France

‡Department of Earth Sciences/Institut Des Sciences de L'Environnement (ISE), University of Geneva, Rue des Maraîchers 13, Geneva 1205, Switzerland

Associate Editor – Victoria Valdez

ABSTRACT

River regulations have resulted in changes in the hydrology and particle budgets of fluvial systems. Since the 19th century, many rivers have been significantly modified to control flood hazards, to gain land from swamp areas for agricultural purposes, and to stabilize river-levels and lake-levels to facilitate navigation. These dramatic changes of the river courses have impacted the sediment budgets and grain-size dissemination along them as well as the sediment distribution at the delta mouths in the downstream lakes, which could lead to slope instabilities. Deposits of such catastrophic lacustrine mass movements caused by delta collapses have been, for instance, observed in Lake Brienz (Switzerland), where relatively thick (0.5 to 1.3 m) and voluminous (>1 million m^3) megaturbidites are stacked in the deep basin witnessing these processes. This study uses sediment cores and seismic data to reconstruct the megaturbidites' history in Lake Brienz. Data reveal that mass-movement deposits, originating from the Aare Delta, one of the two main inflows, have mean ages of 1853, 1905, 1942 and 1996 CE and that they were unprecedented in, at least, half a millennium. The fact that the numbers of floods and earthquakes have not changed radically over this time period implies that human impact is the most likely explanation for these failure events. Therefore, the recurrent delta collapses are attributed to the focused sediment accumulation at the front of the channelized inflow in the proximal delta region, caused by the modification of the Aare River through its straightening and channelization during the late 19th century. These findings indicate that river regulation can affect delta sedimentation, leading to autocyclic delta collapses. Those collapses, in turn, can potentially generate tsunami waves, representing an additional natural hazard for shoreline communities.

Keywords Anthropocene, delta collapse, human-initiated autocyclicity, megaturbidite, slope instabilities.

INTRODUCTION

Human activities significantly influence lacustrine and marine sedimentation. For example, deforestation and land development contribute to increased sediment runoff, while dredging extracts accumulated sediments (e.g. Anselmetti *et al.*, 2007b; Arnaud *et al.*, 2016; Mazure

[1]These two authors contributed equally to this work.

et al., 2024). Significant human activities include infrastructure construction, such as dams and reservoirs, along with river channelization, all impacting natural sedimentation processes. These modifications serve various purposes, including flood control, navigation, agriculture and public health through malaria control (e.g. World Health Organization, 1982). However, such interventions can disrupt the natural sediment transport and deposition processes occurring in rivers and their adjacent basins (e.g. Kesel, 2003; Vörösmarty *et al.*, 2003; Billi & Caparrini, 2006; Anselmetti *et al.*, 2007a; Hein *et al.*, 2019).

Furthermore, one particular concern is the impact of these modifications on deltaic ecosystems. River regulation enhances the accumulation of sediment upstream from hydropower installations (Vörösmarty *et al.*, 1997; Anselmetti *et al.*, 2007a) but also includes sediment extraction in the delta linked to the construction and maintenance of hydropower systems (Lane *et al.*, 2019). Furthermore, the change in the seasonal distribution of river flow due to the exploitation of hydropower structures, which tend to remove natural peaks of high and low river flows, also modifies the river's capacity for transporting sediment (e.g. Yuan *et al.*, 2012). Moreover, river regulation induces changes in the grain-size distribution of transported and sedimented particles, and potentially modifies the spatial distribution of lake deposits (Silva *et al.*, 2019) and the frequency of slope instabilities in delta areas. Understanding the intricate connections between anthropogenic river modifications and delta sedimentation is crucial for evaluating the broader implications on deltaic ecosystems and formulating effective conservation strategies.

Several lacustrine delta collapses have been reported to date (Chapron *et al.*, 1996; Girardclos *et al.*, 2007; Hilbe & Anselmetti, 2014; Praet *et al.*, 2017; Nigg *et al.*, 2021). Their relatively confined extents and smaller dimensions may offer the advantage that they can be studied and quantified on a complete 'source to sink' approach, which is usually not possible on much larger marine counterparts. Nevertheless, gained insights into processes and controls from such lacustrine case studies, such as preconditioning and triggering, can also be applied to marine delta collapses that are also frequently occurring (e.g. Prior *et al.*, 1986; Clare *et al.*, 2016; Terrinha *et al.*, 2019), which all have equal impact on deltaic ecology and hazard potential for shoreline communities and infrastructure.

The resulting deposits of delta collapses comprise two main categories: (i) mass-transport deposits (MTD) directly located at the base of slopes form a wedge-shaped positive morphology with chaotic to transparent seismic facies (e.g. Strupler *et al.*, 2018; Sabatier *et al.*, 2022); and (ii) megaturbidites (or exceptionally large turbidites) corresponding to a thick ponding and seismically homogenous unit (e.g. Leithold *et al.*, 2019; Sabatier *et al.*, 2022). In lakes, as well as in oceans, the lateral non-deltaic and the deltaic instabilities can significantly impact ecosystems in various ways, disturbing aquatic ecosystems and benthic habitats due to increased turbidity and sudden sedimentation, changing water chemistry by locally releasing nutrients and organic matter, reducing oxic levels due to massive release of anoxic pore waters (Girardclos *et al.*, 2007), and producing tsunami-like waves that impact shores. In marine settings, the instance of Nice (France) documents how a newly built harbour extension, constructed at the edge of the International Airport of Nice, collapsed into the Mediterranean waters in 1979 CE, leading to the generation of a tsunami that inundated the cities along the shoreline (Assier-Rzadkieaicz *et al.*, 2000). In lakes, previous occurrences of delta collapses generating tsunamis or seiche effects have been documented in France and Switzerland: Lake Le Bourget in 1822 CE (Chapron *et al.*, 1999); Lake Lucerne in 1687 CE (Hilbe & Anselmetti, 2014); Lake Sils at *ca* 700 CE (Nigg *et al.*, 2021); or Lake Geneva in 563 CE (Kremer *et al.*, 2012).

This study analyses the repeated occurrence of such delta collapses in Lake Brienz (Switzerland) to better constrain their triggers, frequency and volumes. More specifically, this work aims to understand how changes in fluvial sediment supply affect basal stratigraphic architecture of the delta and its geotechnical predispositions to slope instabilities. This knowledge is essential for carrying out a thorough hazard assessment, leading to improved risk-management strategies.

STUDY SITE

Lake Brienz and its catchment

Lake Brienz lies within the frontal range of the Swiss Alps (Fig. 1) in a deep longitudinal valley eroded by the Aare Glacier during the last glaciations. This valley is situated within the Helvetic nappes, consisting of predominantly

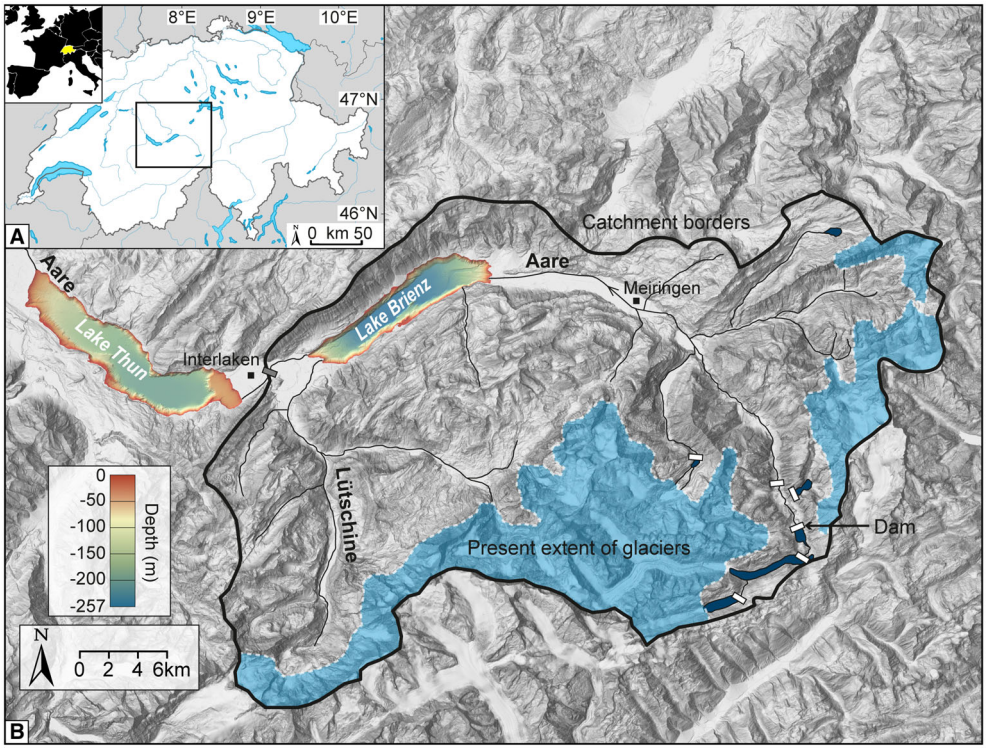

Fig. 1. (A) Location map of Switzerland and Lake Brienz. (B) Shaded relief swissALTI3D digital elevation model (https://map.geo.admin.ch) and high-resolution bathymetric maps of lakes Thun and Brienz (Fabbri *et al.*, 2018, 2021). The catchment area of Lake Brienz is highlighted by the black line. Between 1849 and 1855 CE, a dam was built in Interlaken (grey rectangle; Kurz & Lerch, 1979). From 1929 to 1953, several dams (white rectangles) were constructed and affected the sedimentation in Lake Brienz (Finger *et al.*, 2006; Anselmetti *et al.*, 2007a). The black squares indicate the cities of Interlaken and Meiringen.

calcareous formations from the Cretaceous and Jurassic periods. The lake covers an area of 29.8 km^2 with steep sides and a flat *ca* 250 to 260 m deep basin floor, with a morphology typical of 'fjord-like' valleys (Table 1; Fig. 2). Former reflection-seismic and refraction-seismic studies demonstrated that the lake basement forms two troughs containing 550 m and 300 m of sediment in the west and the east, respectively (Matter *et al.*, 1973). The deepest, glacially-carved basement depression thus lies *ca* 230 m below the modern sea level (Matter *et al.*, 1973).

The catchment area of Lake Brienz covers 1140 km^2 and is characterized by a steep, mountainous landscape partially covered by glaciers (*ca* 19% of total area), with over 50% of its surface lying above 2000 m a.s.l. Most of the lake's catchment is drained by two large rivers, the Aare and the Lütschine (Fig. 1), which both have high water discharge in spring and early summer due to snow melt punctuated by floods throughout the year due to extreme precipitation events. The flow of the Aare River ranged from 24 m^3/s in February to 122 m^3/s in July between 1980 and 2019 (station 2023), whereas the flow of the Lütschine River varied from 3.7 m^3/s in January to 45 m^3/s in July from 1986 to 2019 (station 2109) (Bundesamt für Umwelt BAFU, 2024). These rivers build two large deltas at either end of the lake (Adams *et al.*, 2001). Due to their geologically contrasting catchments, the Aare (predominantly crystalline) and the Lütschine (carbonate-dominated) have distinct silt-sized and sand-sized mineralogical signatures (Sturm & Matter, 1978). A surface-sediment study showed that lateral stream sediment load from small tributaries has little influence on the total lake sedimentation compared to the input of the two main rivers (Sturm, 1976). Lake Brienz is holomictic and ultra-oligotrophic (Nydegger, 1967) with almost exclusively allochthonous clastic input. Sediment distribution is mainly controlled by the varying stratification of river inflows (overflows,

Table 1. Properties of Lake Brienz and its catchment (Finger *et al.*, 2006; Fabbri *et al.*, 2021).

Altitude	564 m above sea level (a.s.l.)
Maximum length	14.2 km
Maximum width	2.8 km
Maximum depth	256 m
Surface area	29.8 km^2
Volume	5.15 km^3
Catchment area	1138 km^2
Mean altitude of the catchment	1951 m a.s.l.
Aare water discharge	1.195 km^3/year (mean 1997–2004)
Lütschine water discharge	0.620 km^3/year (mean 1997–2004)
Aare suspended load (location 'A')	128 kt/year (mean 1997–2004) 176 kt/year (maximum 1997–2004)
Lütschine suspended load (location 'L')	174 kt/year (mean 1997–2004) 242 kt/year (maximum 1997–2004)

interflows and underflows; Sturm, 1976). Particle residence times in Lake Brienz are less than 20 days for fine particles (<4 μm) and less than 4.5 days for coarse (>4 μm) grains (Finger *et al.*, 2006). Lake Brienz can be divided into distinct sedimentation zones, comprising: (i) the proximal delta areas of the Aare and Lütschine, where gravel and coarse sand predominantly accumulate; (ii) the slopes where finely-laminated sediment forms clastic varves; and (iii) the deep basin where hemipelagic fine sediment intercalates with turbidites and megaturbidites (Sturm & Matter, 1978). Based on sediment cores, recent mean sedimentation rates (1996 to 2005 CE) range from 1.2 to 2.3 cm/year in the deep central basin, vary from 1.7 to 2.2 cm/year in the south-western lake basin (near the Lütschine Delta) and from 1.1 to 0.7 cm/year towards the north-east near the Aare Delta. On the lake slopes, sedimentation rates are much lower (0.26 to 0.68 cm/year) as only fine suspended material reaches these parts (Anselmetti *et al.*, 2007a). High-resolution bathymetric data with quasi-four-dimensional seismic data from 2003 to 2018 CE indicates that Lake Brienz exhibits exceptionally high sedimentation rates of 3.0 cm/year in its basin plain, hence surpassing those found in other Swiss lakes (Fabbri *et al.*, 2021).

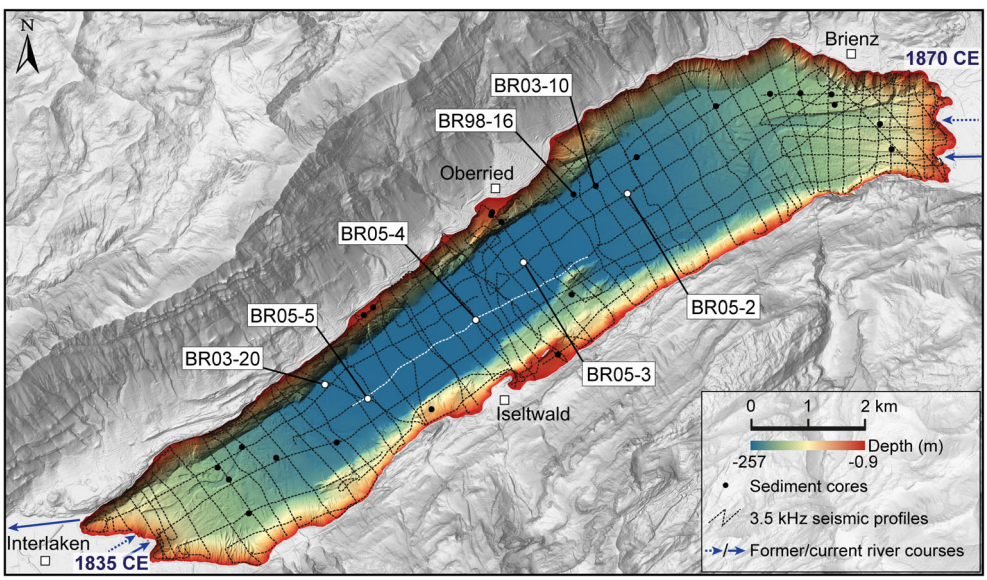

Fig. 2. Shaded relief swissALTI3D digital elevation model (https://map.geo.admin.ch) overlaid by the high-resolution bathymetric map with shaded relief of Lake Brienz (Fabbri *et al.*, 2021). The locations of seismic lines are marked by slashed lines and sediment cores by dots (white dots indicate cores presented in this study). The former and current course of the Lütschine (1835 CE) and Aare (1870 CE) rivers are represented by the dotted and solid blue arrows, respectively. White squares indicate the villages of Brienz, Oberried and Iseltwald, and the city of Interlaken.

History of human impact in the catchment

In 1430 CE, the regulation of fluvial and lake systems began in the Lake Brienz region by constructing a 2 m high dam in Interlaken along the downstream course of the Aare River. This dam was built to facilitate fishing and provide water for a monastery's water mill (Geiser, 1914; Vischer, 2003). The construction of the dam resulted in a lake-level increase of 1.5 to 1.95 m and the formation of extensive swamp areas extending up to Meiringen in the upstream valley ('Haslital') (Kurz & Lerch, 1979; Vischer, 2003). In 1528 CE, during a rebellion associated with the Reformation, the dams were destroyed to allow the Aare River again to flow freely. However, for unknown reasons, the dams were rebuilt soon after that (Geiser, 1914; Vischer, 2003). One of the most severe floods occurred in July 1762 CE, when the Aare River flooded the 12 km long valley from Meiringen to Brienz (Kurz & Lerch, 1979; Röthlisberger, 1991). As a result, the course of the Aare River shifted from its southern to the northern mouth (Mirani, 1764; Kurz & Lerch, 1979; Schulte *et al.*, 2015; Fig. S1), where it remained until it was regulated. The idea of regulating the Aare River and Lake Brienz to gain land from swamps and reduce flood hazards emerged after another significant flood event in 1831 CE, and the decision to undertake the regulation was made in 1834 CE. The project started in 1849/1855 CE with the construction of a new dam in Interlaken (Kurz & Lerch, 1979). The lake level was first lowered after extensive dredging in the Aare riverbed in Interlaken. Between 1866 and 1875 CE, the upstream course of the Aare River was straightened, channelized and rerouted in the alluvial plain from its natural northern mouth to the south, where it currently flows (Fig. 2). Therefore, since the rerouting, the Aare River is only able to discharge its flow at one specific location that is the current river mouth (Fig. 2).

Between 1929 and 1953 CE, four hydropower reservoirs (Grimselsee, Oberaarsee, Räterichsbodensee and Gelmersee) were built in the highest part of the Aare catchment (Grimsel region) acting as sediment traps for coarse-grained material. Since 1940 CE, gravel and sand have been extracted directly from the subaquatic Aare Delta. This mining was initiated to produce the material necessary to construct upstream Grimsel dams, which strongly influence the seasonal Aare discharge pattern (Finger *et al.*, 2006). Overall, these hydropower lakes retain 232 kt/year (Gelmersee not considered) of mostly coarse particles and reduce the total sediment input of the Aare into Lake Brienz by two-thirds (Anselmetti *et al.*, 2007a).

In contrast to the Aare River, the Lütschine River catchment has remained relatively natural with only minor channelization performed on its course. In 1906 to 1908 CE, a dam was constructed to use 6 m^3/s of water for the small Lütschental hydropower station. However, the lower course of the Lütschine River near Interlaken has been subjected to more intensive anthropogenic control. By 1811 CE, its river flowed either to Lake Brienz or directly into the downstream Aare and into Lake Thun. However, in 1835 CE, the Lütschine was directly diverted to the eastern margin of the fan delta and channelized (Schulte *et al.*, 2009). From that time, the Lütschine Delta expanded *ca* 300 m lakeward with a semi-circular morphology (Fig. 2) (Fabbri *et al.*, 2021). Recent observations indicate that the extraction of 25 000 to 30 000 m^3 of gravel per year in this delta is insufficient to prevent it from prograding and becoming unstable (Günter, 2006; Petroni, 2010; Devenish, 2015).

Historic floods in the Lake Brienz region

The list of historical flood events (13th century to present) potentially affecting the Lake Brienz catchment area is established from historical data in Switzerland (Niklaus, 1968; Kurz & Lerch, 1979; Röthlisberger, 1991, 1998; Pfister *et al.*, 1999; Vischer, 2003) and used as a reference catalogue (Table S1). It lists 50 flood events from 1275 to 2005 CE with their date, type of event, and affected regions and river catchments. Twenty of these events are identified as 'major' because they severely impacted rivers, lakes and human society at large geographical extent (Röthlisberger, 1991). For flood events between 1925 and 2005 CE, the date and maximum elevation of flood-related lake-level increase are also indicated (Bundesamt für Umwelt BAFU, 2024). The accuracy of flood description decreases proportionally to the archive's age. For instance, the exact dates of flood events during the 13th to 18th centuries are rarely known, and during the 13th to mid-17th century, only the most significant flood events are reported in historical archives. Historical data reveal that severe floods in Lake Brienz's catchment are generally caused by heavy rain and/or snow melt, usually from June to October.

METHODOLOGY

High-resolution seismic reflection data

Seismic data were acquired in 2003 CE with a 3.5 kHz pinger source (Geoacoustics Limited, Great Yarmouth, UK). A 350 m spaced grid of seismic lines with a total length of 240 km covering the entire Lake Brienz area (Fig. 2) reveals the stratigraphic architecture of the lake subsurface. All seismic data were digitally recorded in SEG-Y format. Data processing was carried out with SPW software, including bandpass filtering (1300 to 1500/6500 to 7000 Hz) and muting the water column's noise. No migration or deconvolution was applied to the data. The recording system was connected to a non-differential GPS with a ±2 to 10 m positioning accuracy. The theoretical vertical resolution is a quarter of the wavelength, i.e. *ca* 0.1 m. Seismic interpretation (i.e. horizon picking and thickness calculation) was done with IHS Markit Kingdom Suite v.2018. The top and bottom seismic horizons of units of interest were used as the upper and lower bounds for thickness/volume determination. The thickness map was then generated by interpolating the horizons in Surfer® (Golden Software LLC, Golden, CO, USA) using a Kriging interpolation. The resulting interpolated grids have a 50 × 50 m spacing, then filtered using a 3 × 3 pixel (150 m) moving average window. A velocity of 1480 m/s was used to convert times to depth in sediments. Finally, the volume was calculated using the 'volume' function in Surfer®.

Sediment-core retrieval and core analysis

Twenty-four sediment cores were collected and analysed from 1998 to 2005 with a gravity corer (1 to 2 m length) and a modified Kullenberg piston-coring system (5 to 10 m length, Kelts *et al.*, 1986). From this set of cores, seven are used for this study (BR98-16, BR03-10, BR03-20, BR05-2, BR05-3, BR05-4 and BR05-5). Gamma-ray attenuation bulk density and magnetic susceptibility were measured using a GEOTEK multi-sensor core logger with a 5 mm resolution (GEOTEK Limited, Daventry, UK). After opening, sediment cores were photographed (*ca* 2 h after), described macroscopically and sampled. To establish core-to-core correlation, visual characteristics and lithological properties were compared.

A composite sedimentary sequence was constructed by identifying marker layers on the overlapping sections, resulting in an 11.3 mcd (metres composite depth) long sequence compiling sections of BR05-2, BR05-5 and BR03-20. While long cores BR05-2, BR05-3 and BR05-4 near the Aare Delta may have potential stratigraphic errors caused by hiatuses below the base of megaturbidites, the upper part of the composite core consists of cores BR03-20 and BR05-05, located in the more south-western part of the basin. These hiatuses did not occur there because the Lütschine side of the lake basin is out of reach of the basal erosion from mass-transport events originating in the Aare Delta (Girardclos *et al.*, 2007). Due to disturbances caused by the coring method at the top of core BR05-5, core BR03-20 is used in the upper part of the sequence (Fig. S2). However, for the lowermost part of the composite core (below the megaturbidites), core BR05-2 was used because it extends over a longer period. Thus, the composite core is composed of core BR03-20 from 0 to the top of MT2 at 86 cmcd, then of core BR05-5 extending from 86 cmcd to a distinguishable event deposit at 796 cmcd (centimetres composite depth), and of core BR05-2 from this depth to the bottom of the composite core (Fig. S2).

Chronology

Terrestrial macrofossils (for example, seeds, needles and wood) were sieved from the wet sediment for Accelerator Mass Spectrometry (AMS) radiocarbon analyses that were performed at the radiocarbon laboratory of ETH/PSI. The ^{14}C ages were calibrated using the Intcal20 calibration curve (Reimer *et al.*, 2020) and expressed on the Common Era (CE) timescale: years before the CE are denoted BCE. The age model is based on: (i) ten radiocarbon ages; (ii) the age of the last two megaturbidites deposited in April 1996 CE (Girardclos *et al.*, 2007) and 1942 ± 2 CE (Anselmetti *et al.*, 2007a); and (iii) the ^{137}Cs activity peaks of 1963 and 1986 CE (Anselmetti *et al.*, 2007a). The age determination with an accuracy of ±2 years is derived from Anselmetti *et al.* (2007a) and is interpolated from two short cores (BR98-16 and BR03-10). The authors extrapolated the sedimentation rate of the sequence between the two ^{137}Cs markers (1963 and 1986 CE) to the top of MT2 with a 10% uncertainty.

The age model has been calculated using the R code package *Bacon v.2.3.9.1* (Blaauw & Christen, 2011). This package applies a Bayesian approach for the age–depth modelling for the entire distribution of the calibrated radiocarbon dates. As the composite core contains sections from different locations within the basin, a boundary was included between each core

section (at 86 and 796 cmcd) in the *Bacon* model so that the memory function is reset (Blaauw & Christen, 2011). The thickness of each 'instantaneous' event deposit (turbidites and megaturbidites) was subtracted from the depth of the composite sediment sequence to create an *event-free depth* scale, which was used to establish a more accurate age–depth model. Event layers were identified on high-resolution core photographs, and a minimal thickness of 0.5 cm was applied to remove thinner event deposits for age modelling, as below this threshold, thinner layers are barely distinguishable from the continuous 'background' sedimentation. The ages of the event deposits were determined by compiling the depth of the event layers in *Bacon* providing the age distribution. Based on this age model, the sedimentation rates of the background sediments, the turbidites, and the whole sediment have been calculated separately for the inter-megaturbidite phases and between MT4 and the bottom of the composite core. The mean recurrence interval and associate uncertainty have been calculated to determine the coefficient of variation (COV) and compute the conditional probability of delta failure in the next 10 (2034 CE), 50 (2074 CE) and 100 (2124 CE) years.

Local intensity of historical earthquakes

The historical earthquake data (Table S2; Fig. S3) were obtained from the ECOS09 catalogue (http://ecos09.seismo.ethz.ch) by selecting a radial range of 200 km around the lake. The intensity at the Aare Delta location (46.74 N, 8.04 E) for each of these historical earthquakes was calculated based on the equations outlined in a prior study (Fäh *et al.*, 2011, appendix E) as follows:

$$\text{Epicentral distances} < 55\ \text{km:}\quad I_{\text{lake}} = -2.8941 + 1.7196 * \text{Mw} - 0.03 * D \tag{1}$$

$$\text{Epicentral distances} > 55\ \text{km:}\quad I_{\text{lake}} = -4.2041 + 1.7196 * \text{Mw} - 0.0064 * D \tag{2}$$

where I_{lake} is the apparent intensity at the lake (Aare Delta) for soil conditions with a vs30 (the time-averaged shear-wave velocity to a depth of 30 m) between 500 and 700 m/s (Fäh *et al.*, 2011), Mw is the moment magnitude from the ECOS09 catalogue, and D is the epicentral distance. The approach used does not account for site-specific ground motion amplification, which can be high and spatially variable in lakes, as shown in a recent study of Shynkarenko *et al.* (2023).

RESULTS

Seismic reflection data

The acoustic penetration in the basin is *ca* 30 to 40 ms two-way travel time (TWT) corresponding to 22 to 30 m sediment depth (assuming a constant mean velocity of 1480 m/s) (Fig. 3). A *ca* 5.5 km long longitudinal seismic line located in the deepest part of the lake at *ca* 260 m depth exhibits two seismic facies (Fig. 3): (i) an intercalation of medium-amplitude reflections with a background composed of laterally continuous low-amplitude reflections (Seismic Facies 1 in Fig. 3); and (ii): a transparent to chaotic seismic facies with ponding geometries (Seismic Facies 2 in Fig. 3). Seismic Facies 2 is intercalated within Seismic Facies 1 and interpreted as megaturbidites intercalated within background deposits based on detailed studies in Lake Brienz (Girardclos *et al.*, 2007). Seismic data reveals two contrasting sequences: (i) a first sequence below 0.362 s TWT (Fig. 3), which exhibits a thick interval dominated by background deposits with the occurrence of only three megaturbidites that are limited in surficial extent (light red in Fig. 3); and (ii) a subsequent thinner sequence above 0.362 s TWT to the lake floor, which is dominated by the four prominent megaturbidites (dark red in Fig. 3) and only relatively thin background intervals. Based on three-dimensional analyses of the seismic profiles, a grid was created to calculate the thickness and volumes of the megaturbidites, indicating a clear difference between the more substantial megaturbidites (MT1–MT4, dark red) and the less significant ones (MT5–MT7, light red) (Fig. 4; Table 2). The older megaturbidites (MT5–MT7) exhibit smaller volumes (Table 2), ranging from 0.58 to 0.94 (10^6) m^3, and appear thinner and do not extend towards the south-western part of the profile (Figs 3 and S4). In contrast, the four recent megaturbidites (MT1–MT4) show larger volumes, varying from 1.25 to 2.35 (10^6) m^3 and extend over larger areas (Table 2; Fig. 4).

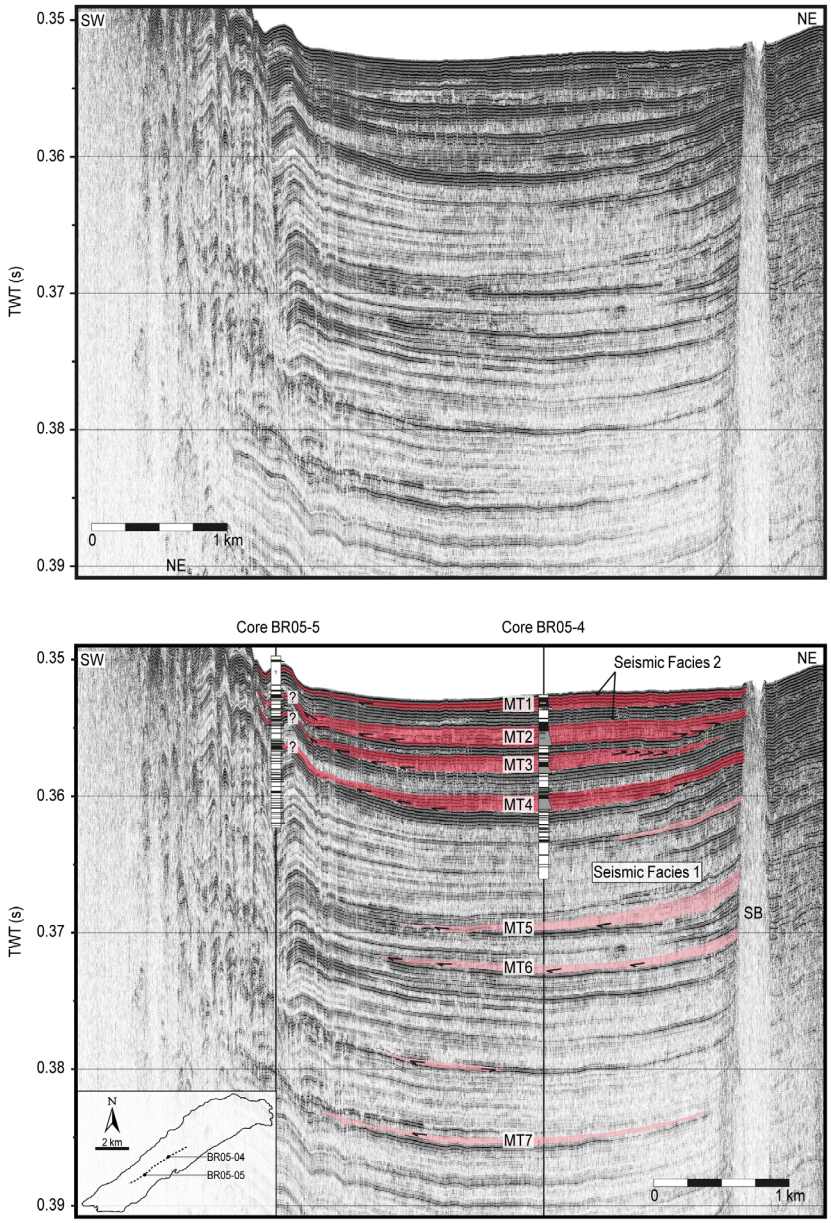

Fig. 3. 3.5 kHz longitudinal seismic section in the raw and interpreted version above and below, respectively, with an inset of its location in Lake Brienz. Two main seismic facies can be discerned: Seismic Facies 1 = laterally continuous low to medium amplitude reflections; Seismic Facies 2 = transparent to chaotic seismic facies with ponding geometries, interpreted as megaturbidites (MT). The thickest and most recent megaturbidites are drawn in dark red (MT1–MT4), while the less extensive and older ones are marked in light red (MT5–MT7). Side blanking is denoted as SB. Black arrows indicate the seismic terminations (onlaps, truncations) used to delimit the megaturbidites. The upper part of core BR05-05 is disturbed, making it challenging to confidently correlate this sediment sequence with seismic reflections but sediment core BR05-4 fits well to the corresponding seismic facies.

Fig. 4. Thickness maps of the seven megaturbidites MT1 to MT7 – panels (A) to (G) – derived from seismic data superimposed on the shaded relief swissALTI3D digital elevation model (https://map.geo.admin.ch) and the high-resolution bathymetric map (Fabbri *et al.*, 2021). The megaturbidite volume is indicated in the upper right corner of each panel. The location of four long sediment cores (BR05-02 to BR05-05) is marked with black dots.

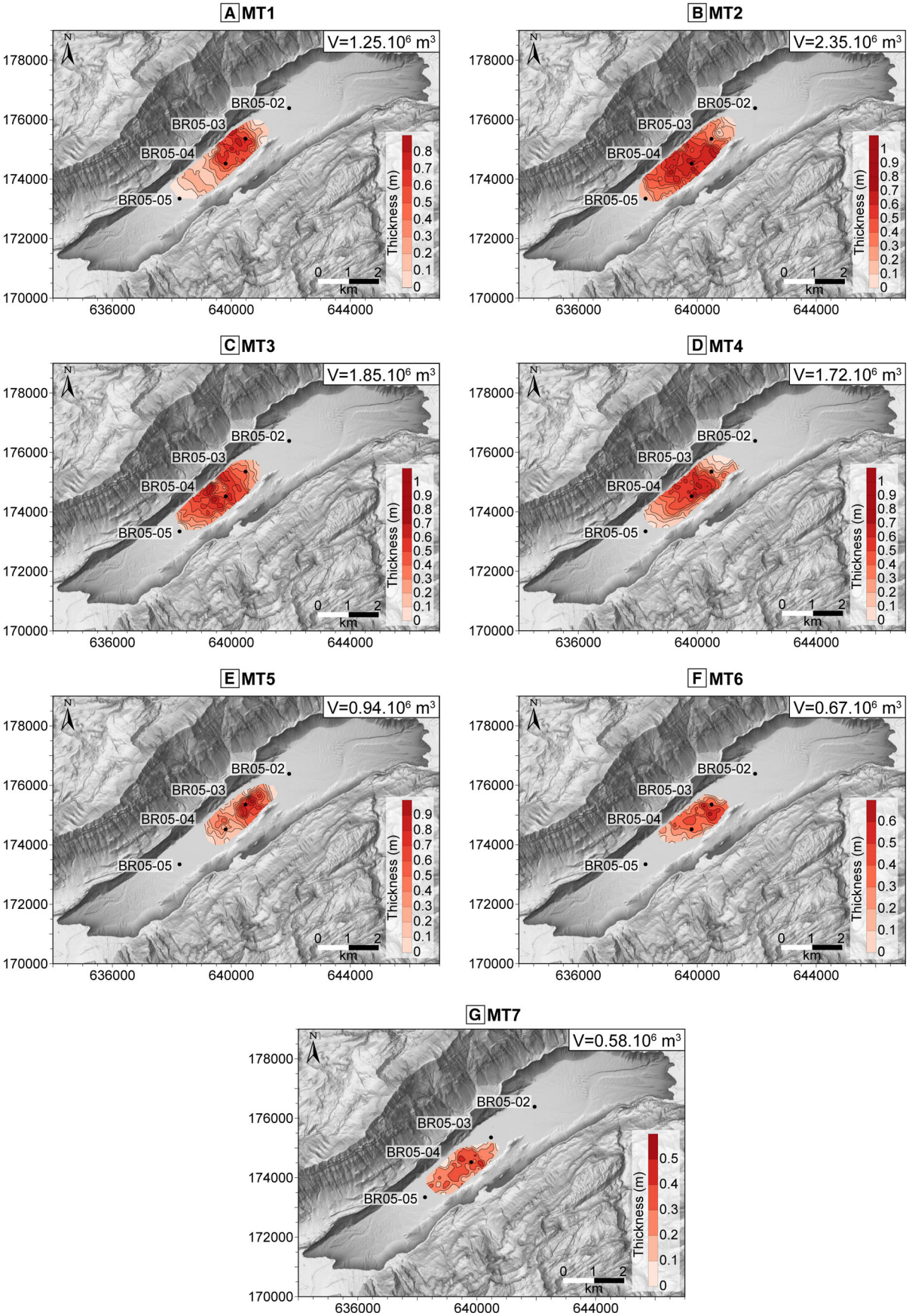

Table 2. Volume and surface area of each megaturbidite (Seismic Facies 2) (Fig. 3) computed from seismic data grid (Fig. 2).

Seismic Facies 2 units interpreted as megaturbidites (Fig. 3)	Volume ($\times 10^6$ m^3)	Surface area (km^2)
MT1	1.25	2.54
MT2	2.35	3.52
MT3	1.85	3.14
MT4	1.72	3.34
MT5	0.94	2.37
MT6	0.67	2.03
MT7	0.58	2.19

Sediment record

The studied four long cores, BR05-2 to BR05-5, collected in the deep lake basin (*ca* 260 m depth), are situated along the longitudinal axis of the lake (Figs 2 and S4). They show well-layered clastic sediment of highly varying colour and texture, which can be correlated from core-to-core throughout the basin (Fig. 5).

Lithotypes

The sediment record comprises three main lithotypes. The following description is based on core BR05-04 for which the density and magnetic susceptibility are displayed (Fig. 5).

Lithotype 1: Fine laminated/layered silt to clay (interpreted as background sediment)
Lithotype 1 sediment consists of millimetre-thick clayey silt layers alternating with graded silt-sized to fine sand-sized layers that are less than 5 mm thick. The bulk density of these sediments fluctuates around 1.5 g/cm^3 and the magnetic susceptibility varies between 10 and 20×10^{-5} SI units (Fig. 5). This lithotype is interpreted as hemipelagic clastic background sediments and forms the event-free composite record.

Lithotype 2: Graded layers (interpreted as event deposits)
Subtype 2a: Graded silty-sand layers (interpreted as turbidites). Subtype 2a comprises graded layers with a thickness of 0.5 to 26 cm. They typically show a slightly graded sandy layer rich in organic debris at the bottom, mainly composed of terrestrial macrofossils such as pieces of leaves, roots and bark. The upper part of each layer is usually a well-graded silt layer capped by a light-coloured clayey cap. One of the thickest of these layers occurs in core BR05-04 (10.5 cm at 545 cmcd) and exhibits a density peak of up to 1.7 g/cm^3 at its coarsest-grained base, associated with a maximum magnetic susceptibility of 19×10^{-5} SI units, which both gradually decrease towards the top of the layer. However, this pattern in density and magnetic susceptibility is not visible in all Subtype 2a layers, likely due to the measurement interval of 5 mm.

These graded layers are interpreted as turbidites mainly generated by high-discharge flood events in one of the first detailed sedimentological studies in the lake, based on 140 surface samples and 80 sediment cores (Sturm & Matter, 1978). Based on the core-to-core correlation, the conclusions herein match those of Sturm & Matter (1978); these turbidites can be subdivided into two categories with different basinal trends in grain size and bed thickness (Fig. 5). Turbidites that become thicker and coarser towards the north-east are interpreted as flood deposits from the Aare River, while turbidites becoming thicker and coarser towards the south-west are interpreted as flood deposits from the Lütschine River. This interpretation is supported by the sediment colour of the turbidites, with grey indicating sediment originating from the crystalline-dominated Aare River catchment, and black indicating sediment coming from the carbonate-dominated Lütschine River catchment (Sturm & Matter, 1978). It is not excluded that certain turbidites may result from localized mass-wasting events. Conducting a dedicated study to investigate their timing and correlation with historical archives could provide valuable insights into addressing this question. Subtype 2a layers have been removed from the age modelling, because they represent rather instantaneous event layers.

Subtype 2b: Thick graded sandy layers (interpreted as megaturbidites). Subtype 2b occurs in four exceptionally thick graded layers (56.5 to 128 cm thickness; Fig. 6) that can be identified in the cores of Lake Brienz labelled downcore from 'a' to 'd' (Figs 5 and 6). They consist of two distinct parts: (i) a bottom section mainly consisting of greyish upward fining sand characterized by high but upward decreasing density (from 1.9–2.0 to 1.5–1.7 g/cm^3) and magnetic susceptibility (from 19–22 to 15–17 $\times 10^{-5}$ SI units) values (Fig. 6, grey colour); and (ii) an upper part consisting mainly of rather homogeneous silt topped

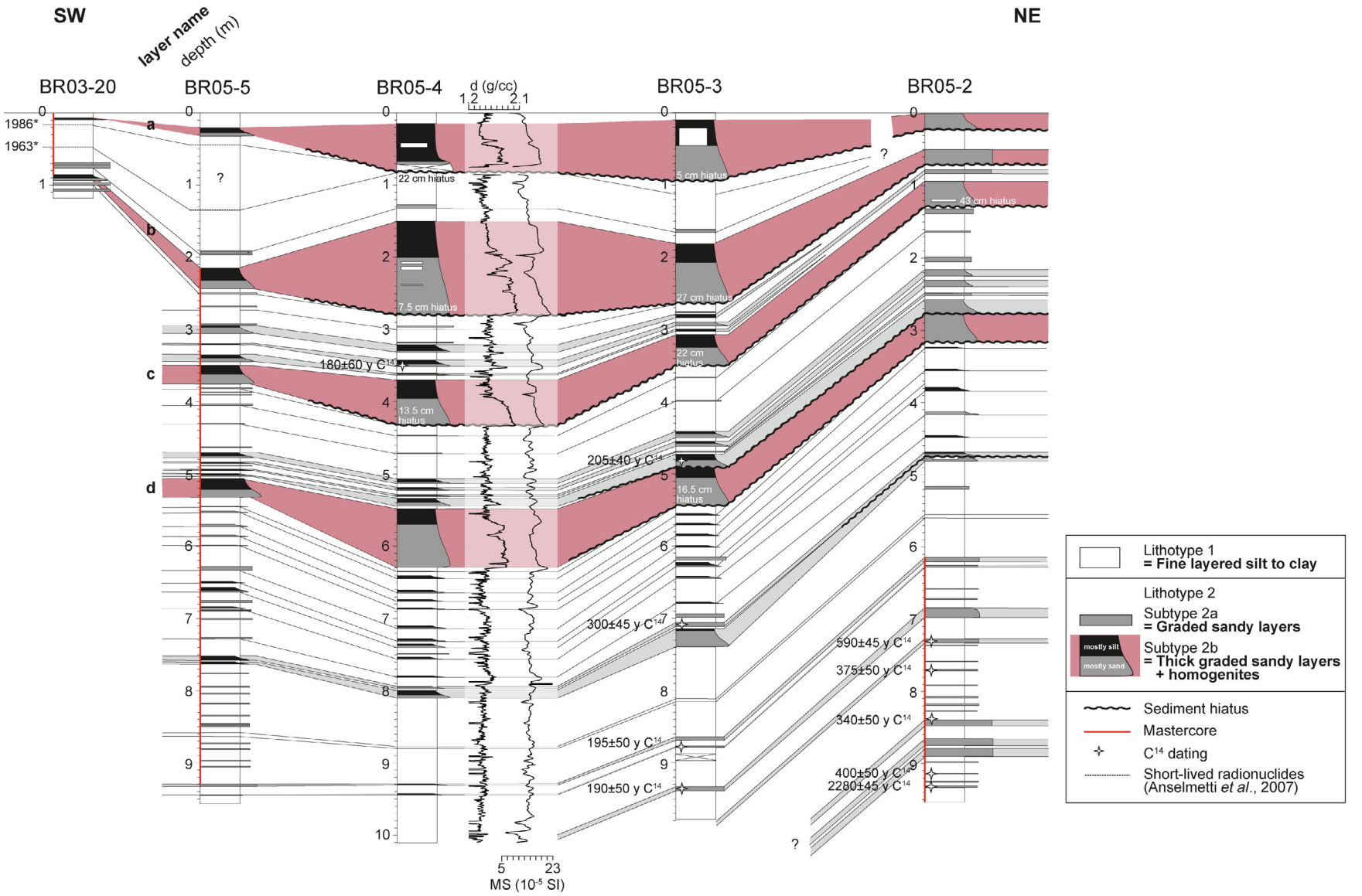

Fig. 5. Correlation between the four long cores (BR05-02, BR05-03, BR05-04 and BR05-05) and the short core BR03-20 allowing the construction of the composite core. The red vertical lines in the different core sections (BR03-20, BR05-05 and BR05-02) indicate the sections belonging to the composite core. The correlation between lithotype 2b beds (megaturbidites) is marked in red. A limited number of lithotype 2a layers (turbidites) are highlighted and correlated in grey, emphasizing the general correlation. The white colour points to lithotype 1. The density and magnetic susceptibility curves are displayed for core BR05-04. Sediment hiatus (curvy black line) and C^{14} dating samples (star) are pointed when present.

by a white clayey cap. This upper part is characterized by lower and constant density (*ca* 1.5 g/cm^3) and magnetic susceptibility (*ca* 16×10^{-5} SI units) values (Fig. 6, black colour). Three of the four megaturbidites ('a', 'b' and 'd') in core BR05-04 partly include clasts of hemipelagic sediment at their base (Fig. 6). Subtype 2b layers are also excluded from the age modelling.

Core-to-seismic correlation

The core-to-seismic correlation was done by comparing the sedimentological observation and the density values with the seismic data, assuming a mean velocity of 1480 m/s. The core-to-seismic correlation reveals that the core sections with Lithotype 2b coincide with Seismic Facies 2 characterized by chaotic facies and wedging and/or ponding geometries that were identified in the seismic data as megaturbidites (MT1–MT7). They are interpreted to be the product of particle transport in suspended flows originating from major instantaneous mass movements generated in the delta (Fig. 3). Seismic Facies 1 (laterally continuous low-amplitude reflections) constitutes the background sediments (Lithotype 1) and turbidites (Lithotype 2a).

Detailed analysis of the sediment stratigraphy through core-to-core correlation in the basin shows that megaturbidites often have erosive bases that cause sediment hiatuses in the distal Aare Delta and the deepest parts of the lake pointing to a mixed (or composite) flow rheology (Talling *et al.*, 2004, 2012; Girardclos *et al.*, 2007; Haughton *et al.*, 2009). This provides evidence of the transformation from a cohesive to a non-

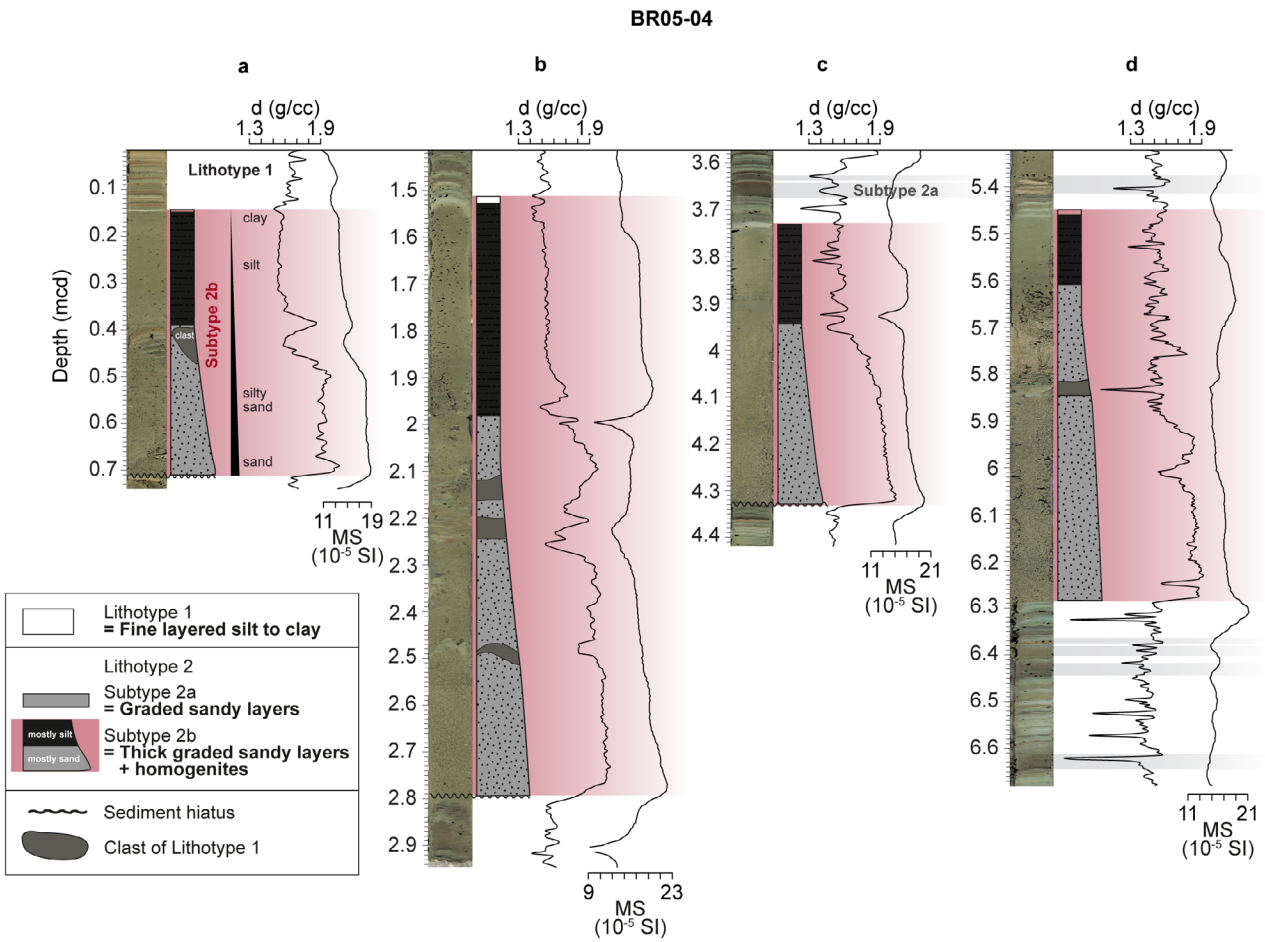

Fig. 6. Lithological and petrophysical characteristics of the four most recent megaturbidites, labelled from 'a' to 'd' (Core BR05-04, also Fig. 5). From left to right: core picture, lithology column (fine left, coarse right), bulk density and magnetic susceptibility profiles. Sediment clasts of background sedimentation (Lithotype 1) are present in the megaturbidites (Lithotype 2b).

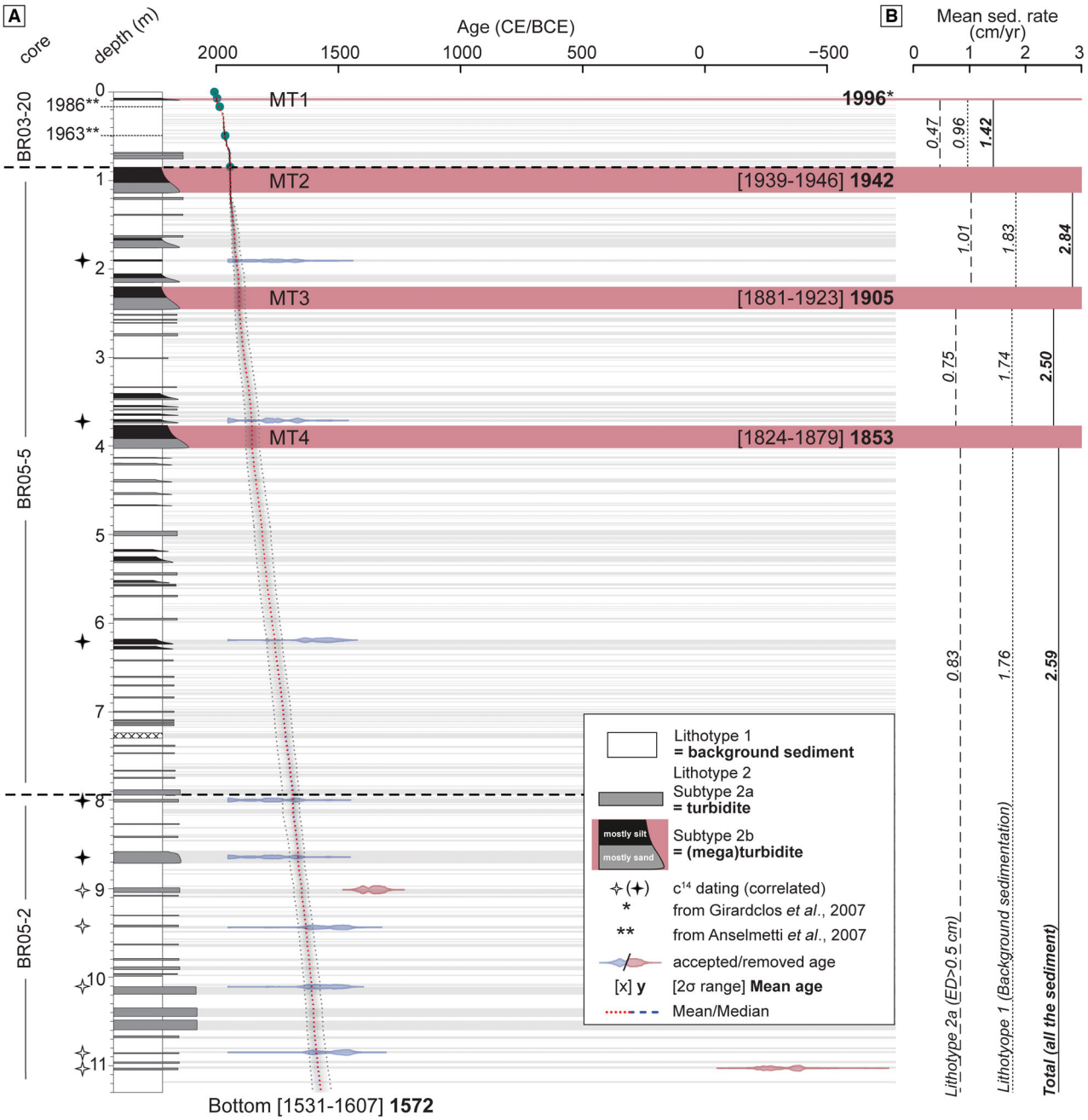

Fig. 7. (A) Age model of the composite core (consisting of cores BR03-20, BR05-5 and BR05-2). The dashed black lines represent the transitions from one core section to another in the composite core. The light-grey horizontal bars represent the thin turbidites (thickness larger than 5 mm). The red horizontal bars represent the megaturbidite beds. (B) Sedimentation rates (cm/year) are indicated for three categories: the background sedimentation (Lithotype 1), the turbidites (Subtype 2a), and the whole sediment calculated in between the occurrence of each megaturbidite (Lithotype 2b). Note that megaturbidite 'MT1' is in the composite section only a thin layer, as its thickest expression in more basinal cores was disturbed.

cohesive flow by the deposition of debrite–turbidite beds during the same flow event. The thicknesses of the hiatus are estimated from detailed core-to-core correlation and vary from centimetre to decimetre-scale (Fig. 5).

Age–depth model and ages of the megaturbidites

The calculated age model indicates that the composite core covers a time range from 2003 at the top

Table 3. Accelerator Mass Spectrometry (AMS) radiocarbon age determination of terrestrial macrofossils from Lake Brienz sediment samples. Ages rejected in the model are given in italic letters (Fig. 7).

Samples					AMS radiocarbon age	
Core section	Laboratory reference	Section depth (cm)	Composite depth (cm)	$\delta^{13}C_{PDB}$ [‰]	Conventional [^{14}C year BP]	Calibrated 2σ [CE]
BR05-4-7	ETH-30850	80	1.945	−25.3 ± 1.1	180 ± 60	1645/(>1950) (95.4%)
BR05-3-6	ETH-30849	116	3.730	−22.2 ± 1.1	205 ± 40	1637/1699 (26.9%) 1722/1814 (48.2%) 1834/1886 (6.0%) 1909/(>1950) (14.3%)
BR05-3-3	ETH-30848	16	6.295	−25.5 ± 1.1	300 ± 45	1472–1664 (94.0%) 1784–1794 (1.5%)
BR05-3-2	ETH-31130	92	8.050	−24.6 ± 1.2	195 ± 50	1638/1895 (79.7%) 1902/(>1950) (15.7%)
BR05-3-1	ETH-31131	39	8.745	−22.0 ± 1.2	190 ± 50	1641/1895 (79.3%) 1902/(>1950) (16.1%)
BR05-2-3	*ETH-31132*	*45*	*9.040*	*−25.1 ± 1.2*	*590 ± 50*	*1294/1425 (95.4%)*
BR05-2-2	ETH-31134	2	9.485	−23.1 ± 1.2	375 ± 50	1444/1636 (95.4%)
BR05-2-2	ETH-31133	70	10.160	−25.8 ± 1.2	340 ± 50	1455/1646 (95.4%)
BR05-2-1	ETH-31455	56	10.915	−25.8 ± 1.2	400 ± 50	1428/1529 (59.5%) 1540/1635 (36.0%)
BR05-2-1	*ETH-30847*	*73.5*	*11.090*	*−24.7 ± 1.1*	*2280 ± 45*	*−408/−342 (41.4%)* *−321/−201 (54.0%)*

to a mean maximum age of 1572 ± 38 year CE (Fig. 7A; Table 3) at the base. The age of 1996 CE for MT1 is retrieved from the literature (Girardclos *et al.*, 2007). Based on the age–depth model of the composite core with a 2-sigma uncertainty, the age ranges of the three older megaturbidites could be estimated as 1939 to 1946, 1880 to 1924 and 1822 to 1881 CE, with mean ages of 1942, 1905 and 1853 CE, respectively (Fig. 7A). The age model also highlights the fact that the estimated average recurrence interval of MT1 to MT4 events is 47.7 ± 13.08 year (Figs 7 and S5), with a coefficient of variation (COV) of 0.27, low enough to attempt a forecast for the next megaturbidite event. Based on a normal distribution of the recurrence interval, the probability of a megaturbidite event happening in the next 10 (2034 CE), 50 (2074 CE) and 100 (2124 CE) years are respectively 22.92, 98.97 and >99% (Fig. S5). However, it is important to note that a small number of events (in the present case, four) can lead to an underestimation of the COV value, so these probabilities should be taken with caution (e.g. Kempf *et al.*, 2018; Williams *et al.*, 2019; Kempf & Moernaut, 2021).

The mean sedimentation rates of the background sediments (Lithotype 1), the turbidites (Lithotype 2a) and the whole sediment has been calculated separately for the inter-megaturbidite phases (Fig. 7B; Table S3). These rates are quite stable from the bottom of the core to the megaturbidite MT2, with *ca* 1.78 cm/year for the background sedimentation (Lithotype 1), 0.86 cm/year for the turbidites (Lithotype 2a) and 2.6 cm/year in total. Then, the mean sedimentation rate drops after the megaturbidite MT2 to 0.96 (Lithotype 1), 0.47 (Lithotype 2a) and 1.42 cm/year (whole sediment), respectively. This last drop in accumulation rate is likely an artefact due to the change of sediment section from core BR05-05 to core BR03-20, which is closer to the shore (Fig. 2). Extrapolating a similar sedimentation rate of 2.6 cm/year to the entire sediment sequences imaged by the seismic reflection data and using a p-wave velocity of *ca* 1480 m/s, the base of the seismic profile in Fig. 3 at 0.39 s TWT is estimated to date back to around 950 CE.

This extrapolation of the age model allows not only to give approximate ages for MT5 (16th century CE), MT6 (15th century CE), and MT7 (12th century CE) (Fig. 3) but also to date the 'quieter' phase when megaturbidites are less extensive and less frequent. In summary, during the first *ca* 900 years

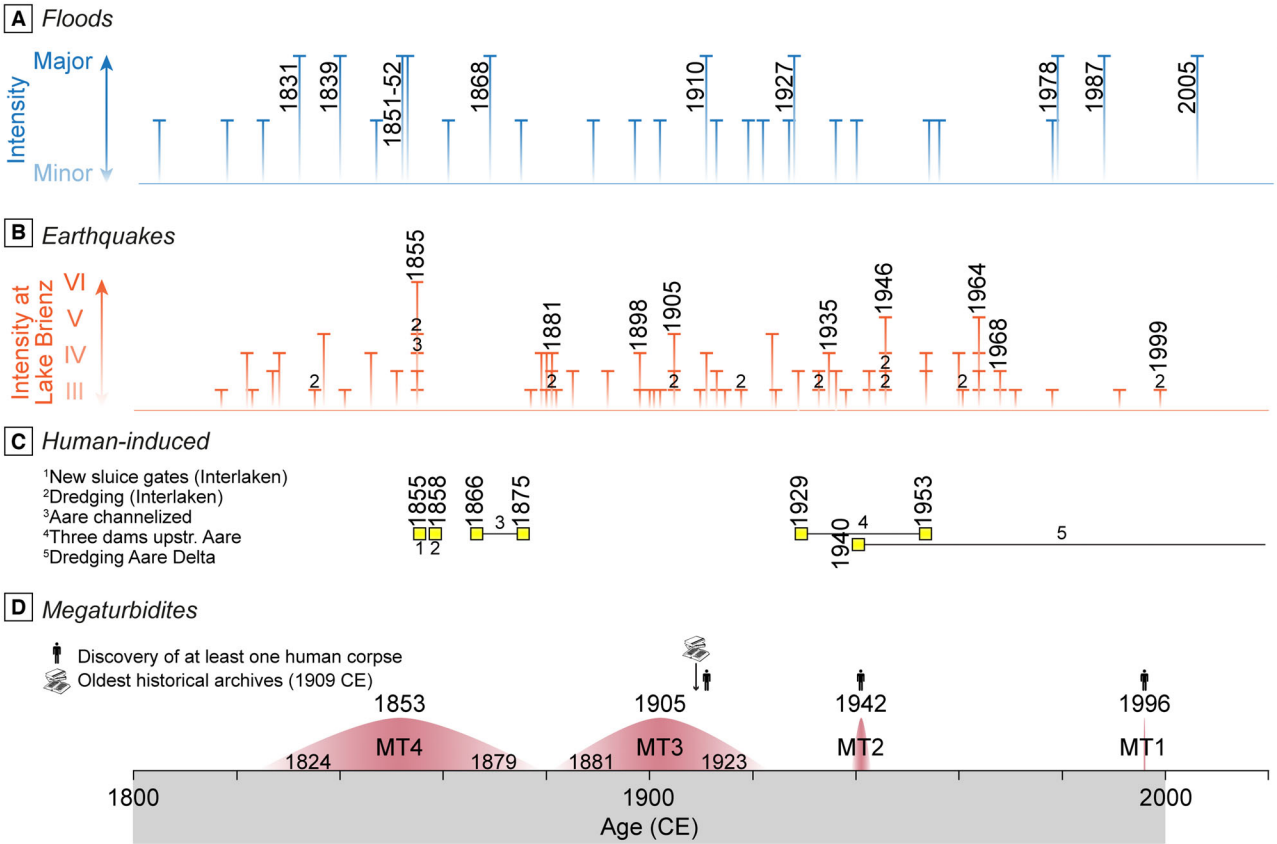

Fig. 8. Chronological representation of the age range of: (A) historical floods and their relative intensities (Table S1). (B) Historical earthquakes in the region, having seismic intensities greater than III at the Aare Delta location, were determined using the equation of Fäh *et al.* (2011) (Table S2). The indices represent the number of earthquakes when multiple events occurred within the same year. (C) Human-induced impacts that affected Lake Brienz's catchment. (D) Megaturbidites and their 2-sigmas age uncertainties and mean age (Fig. 7). The grey box indicates the location of the timescale in Fig. 9B. The earliest archive from the Oberländer Tagblatt newspaper that can be used to determine whether a body has been found or not date back to 1909 CE (https://www.e-newspaperarchives.ch).

of the sedimentary record studied in this work (i.e. from the 10th century to the 19th century CE), only three megaturbidites occurred. Assuming a 100 year uncertainty range for the age of MT5, MT6 and MT7, this study has a mean recurrence interval of 234 ± 80 years. In contrast, a cyclic pattern with a mean recurrence interval of less than 50 years (*ca* 4.7 times less) started in the 19th century (Figs 3 and 8) with MT4 in 1853 CE.

DISCUSSION

Sediment source and origin of the megaturbidites

The most recent megaturbidite (MT1) has been studied in detail by Girardclos *et al.* (2007). The authors presented direct and sedimentological observations pointing to a slope failure in the proximal Aare Delta area.

1 The sand content decreases longitudinally from the north-east to the south-west, like for MT2, MT3 and MT4 in cores BR05-2 and core BR05-5 (Fig. 5).

2 The grey colour indicates remobilized particles from the Aare River catchment, as previously described in Sturm & Matter (1978).

3 The core-to-core correlation indicates sediment hiatus beneath megaturbidite beds in the north-east and central parts of the basin, pointing to increased erosion in these locations (Fig. 5). These areas were likely situated more proximally to the source. Additionally, the presence of sediment clasts originating from a more Aare-proximal location in the megaturbidites

(Fig. 6) indicates that eroded clasts were still being incorporated during the mass/flow transport at this location corresponding to a mixed (or composite) flow rheology (Talling *et al.*, 2004, 2012; Girardclos *et al.*, 2007; Haughton *et al.*, 2009).

4 In 1996 CE, a corpse was discovered floating on the northern shore of Lake Brienz near Oberried after being released from the sediment by the delta failure (Girardclos *et al.*, 2007). Historical chronicles that on 19 September 1942 CE, a floating corpse was also discovered in the same location (Oberländer, 1942). There is therefore a very likely link between the discovery of the corpse and MT2 with a mean age of 1942 CE. As proposed by Girardclos *et al.* (2007), the counter-clockwise circulation of the lake (Nydegger, 1967, 1976; Sturm, 1976) would indeed carry the floating bodies to the northern shore, where they have been found twice. The same applies to MT3, when mutilated bodies of a man and a woman, the thigh of a third person and several animal carcasses were found in the lake near the delta mouth of the Aare in 1913 CE. This evidence has already been interpreted to indicate a delta failure at that time: "Man vermutet, daß bei der Aaremündung ein sogenannte Sandritt niedergegangen sei, so daß die Leicher bloßgelegt wurden." (Oberländer, 1913). It therefore reinforces the hypothesis of the Aare Delta as the origin of the megaturbidites. The oldest historical record is from 1909 CE, therefore it is not possible to investigate whether any bodies were also discovered at the time of MT4 deposition (Fig. 8D).

The quasi-similarity of the four most recent megaturbidites in terms of sedimentology and geometry, in addition to the discovery of the resuspended corpses in three of these cases indicates that the sedimentary flows forming MT1 to MT4 all originate from the Aare Delta, as has been demonstrated explicitly for MT1 (Girardclos *et al.*, 2007).

Within the seismic reflection profiles, seven megaturbidites are observed, where the most recent four have larger volumes than the older ones (Table 2; Fig. 4). However, it is essential to acknowledge that the volumetric results obtained from seismic data might underestimate the true extent of megaturbidites (Fig. 4). For example, at core BR05-02 and BR05-05 locations, the seismic line does not indicate the presence of megaturbidites MT1 to MT4 (Figs 3 and S4). However, the sediment cores do confirm the presence of those megaturbidites. In cores BR05-05 and BR05-02, the thicknesses of the megaturbidites span from 11 to 28 cm and 21 to 39.5 cm, respectively (Fig. 5). The vertical resolution of the seismic 3.5 kHz source is theoretically limited to approximately 10 cm, which should have been sufficient to observe them. Nevertheless, the area is marked by a weaker penetration of the acoustic signal in the seismic data, which has affected the interpretation.

In addition, the older three megaturbidites (MT5–MT7) happened in 900 years, while the most recent (MT1–MT4) occurred in the past 200 years. This points to an average recurrence rate of 47.7 ± 13.08 year, where the timing between MT3 and MT2 of 37 years is shorter than the period between MT4 and MT3 and MT2 and MT1, with 52 and 54 years, respectively. Consequently, the 1996 CE event is not isolated but has historical antecedents. This analysis of the seismic reflection data reveals the existence of at least six other occurrences, all originating from the Aare Delta. However, the exact reasons behind these delta collapses remain ambiguous and need further investigation. This study investigates potential causes based on the dated megaturbidites in the upcoming section.

Triggers and causes of megaturbidites

Short-term triggers

Delta failures can be caused by different short-term and long-term triggers and causes, such as earthquakes, sediment loading, changes in water levels, cyclic loading from waves and biochemical processes (for example, the generation of pore gases) (e.g. Coleman & Prior, 1988; Hilbe & Anselmetti, 2014; Praet *et al.*, 2017). A previous study in Chilean lakes showed that, in seismically active areas, delta collapses are usually triggered by seismic shaking, because earthquakes occur more often, preventing deltas from being overloaded by sedimentation (Van Daele *et al.*, 2015). In the case of Lake Brienz, which is in a seismically much less active area, seismic shaking might or might not be the primary trigger. In fact, for MT1, it has been shown that the collapse occurred spontaneously from sediment overloading (Girardclos *et al.*, 2007).

Megaturbidite 2 occurred in 1942 ± 2 years CE based on Anselmetti *et al.* (2007a), and between 1939 and 1946 CE (mean age: 1942 CE) based on age modelling in this study. It has mobilized the largest sediment volume (2.35×10^6 m^3) among

the megaturbidites of this study (Table 2; Fig. 4B). As mentioned in the *Sediment source and origin of the megaturbidites* section, historic chronicles indicate that on 19 September 1942 CE, a floating corpse was discovered on the northern shore of Lake Brienz (Oberländer, 1942) so the timing of the MT2 can be narrowed to 1942 CE if those events are related to one another. Within 1942 CE, no major flood was reported in the Aare Valley (Fig. 8A), but two successive Mw = 3.5 earthquakes occurred on 27 and 28 August 1942 CE, with intensities of $II^{1/2}$ at the lake, *ca* 20 days before the discovery of the corpse (Table S2). This coincidence could suggest that the delta was near to overloading at that time and became triggered by one of these weak earthquakes (for example, due to a change in the pore-water pressure distribution), although spontaneous failure is equally likely. Two other earthquakes occurred in 1943 CE with moment magnitudes of 5.1 and 5.4 and intensities of III at the lake, and could also be considered as potential candidates. Compared to areas with high seismic activity such as Chile and Alaska, where earthquake-triggered delta failures occur at intensities $>V^{1/2}$ (e.g. Moernaut *et al.*, 2014; Vanneste *et al.*, 2018), here the authors consider that even smaller earthquakes might be able to trigger delta collapses, in particular when the delta is overloaded and near-failing. Together with the evidence of the released corpse, the weak 27/28 August earthquakes are thus considered to be the most likely triggers to have caused the failure of the overloaded delta resulting in MT2 (Fig. 8B; Table S2).

Megaturbidite 3 is dated between 1881 and 1923 CE (mean age; 1905 CE), from the age modelling at 2-sigma uncertainty (Fig. 7). The sediment volume of this megaturbidite is $1.85 \times 10^6\ m^3$ (Table 2; Fig. 4C). A major flood of national importance occurred in 1910 CE caused by heavy rainfall and snow melt, which significantly increased the sediment input at the Aare Delta (Pfister *et al.*, 1999, Fig. 8A). In addition, 26 earthquakes with intensities ranging from III to IV at the lake occurred within this interval (Fig. 8B; Table S2) so that an earthquake trigger cannot be excluded. However, similar to MT1 and MT2, the discovery of human and animal corpses on 21 September 1913 CE, supports a date shortly before this finding as the age of MT3.

Megaturbidite 4, deposited between 1824 and 1879 CE (mean age: 1853 CE; Fig. 7), has a volume of $1.72 \times 10^6\ m^3$ (Table 2; Fig. 4D). During this interval, several significant floods occurred (1831, 1839, 1851 to 1852 and 1868 CE) due to heavy rainfall and snow melt (Pfister *et al.*, 1999, Fig. 8A) further loading the delta. Additionally, seismic activity may have played a role, as 26 earthquakes occurred during that period. In particular, an earthquake swarm occurred in 1855 CE comprising a Mw = 6.2 event *ca* 60 km from the Aare Delta that had an intensity of VI at the lake (Fig. 8B), which is the earthquake with the highest local intensity during this period of 75 years (Table S2).

While the aseismic trigger for MT1 is confirmed, attributing a seismic trigger to MT2 to MT4 remains speculative. Overall, floods providing sediments are considered as the long-term cause for gradually overloading the delta's slopes. Earthquakes of various intensities may represent the final trigger for delta collapses, depending on the degree of slope charging, but if overloading exceeds the static stability, the delta may also fail without an external trigger. However, as floods and earthquakes have occurred throughout the centuries, they cannot explain the increase in more frequent delta failures since 1850 CE in Lake Brienz. Tectonic boundaries have not changed during this period and no specific earthquake swarms have been detected since 1850 CE that could explain the recurring megaturbidites (ECOS catalogue). Moreover, only small-scale variations have been observed in the flood records over the centuries (Schulte *et al.*, 2015). Palaeoflood records consistently show intense flooding over the past 500 years (Pfister *et al.*, 1999; Schulte *et al.*, 2015). The 20th century has been rather characterized by an absence of major floods, the so-called 'disaster gap' (Pfister, 2009). The fact that three of the four megaturbidites occurred during the 20th century requires additional controls on megaturbidite generation.

Long-term causes

Since the 19th century, major climate changes and human-induced catchment modifications have affected the sediment accumulation in the Aare Delta. First, the Little Ice Age may have intensified erosion and sediment production within the catchment area, potentially resulting in higher sedimentation rates in Lake Brienz. Glacier retreat begins around 1850 to 1870 CE (e.g. Masson-Delmotte *et al.*, 2013). However, the sedimentation rate remains constant at *ca* 2.6 cm/year from 1572 to 1942 cal. CE (Fig. 7) so that the Little Ice Age climate deterioration

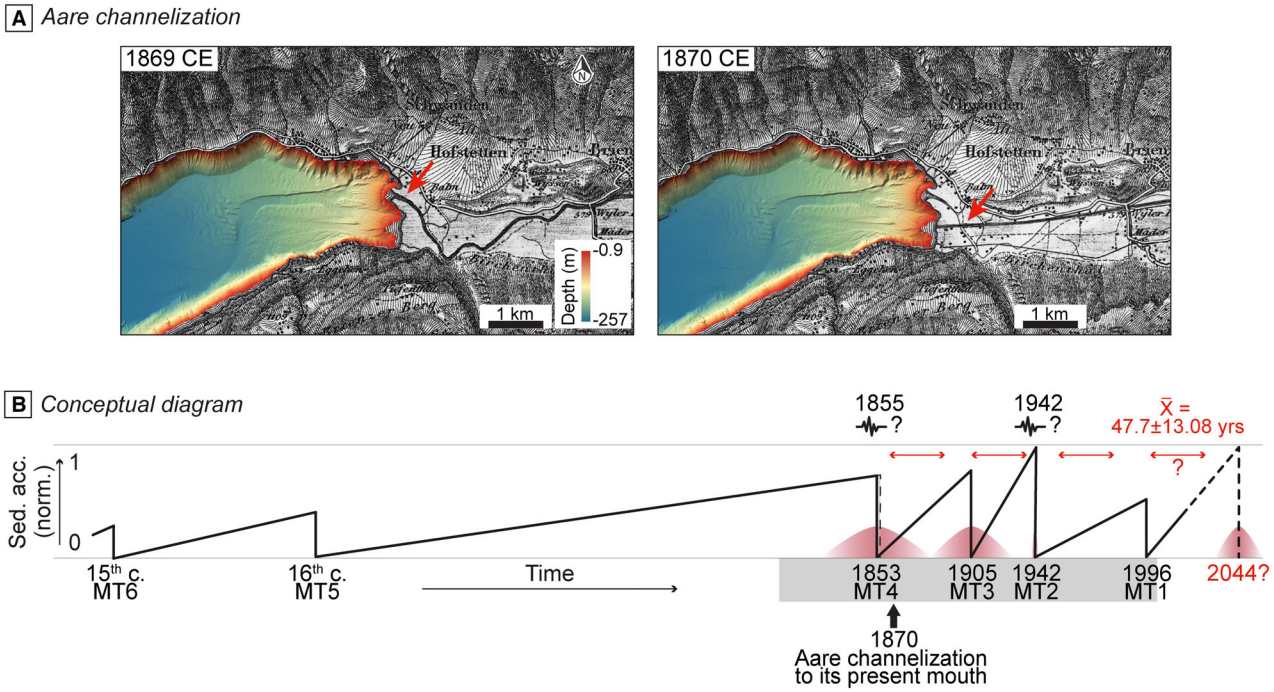

Fig. 9. (A) Historical maps showing the north-eastern region of Lake Brienz and the Aare River's straightening and channelization between 1869 CE (left) and 1870 CE (right) (source: https://map.geo.admin.ch). (B) A conceptual diagram illustrating the potential sediment accumulation threshold on the Aare Delta before and after the river correction in 1870 CE. The vertical scale represents the volume of each megaturbidite, normalized by the maximum volume (MT2; Fig. 4). The black line shows that the delta slope slowly recharges until it collapses, repeatedly generating megaturbidites. However, this internal sedimentary autocyclicity can be altered when earthquakes or major floods act as external triggers. The red shading indicates the age uncertainties associated with each megaturbidite, and the grey box indicates the location of the timescale in Fig. 8D.

appears with only minimal impact on the particle budget. As previously mentioned in the *Age–depth model and ages of the megaturbidites* section, the apparent drop in sedimentation rate observed after 1942 cal. CE (i.e. after MT2) is due to the change of sediment section from BR05-05 to BR03-20, which is at a more distal location from any sediment source and is thus considered an artefact (Figs 2 and 7). Overall, the effect of the Little Ice Age on the sedimentation's history may be small and is not considered as a relevant process to explain the higher frequency of delta failures.

Towards the end of the Little Ice Age, between 1866 and 1875 CE, humans start to actively modify the course of the Aare River by straightening and channelling it from north to south (the significant change is carried out in 1870 CE; Fig. 9A). These modifications terminate the natural fluctuations of the Aare mouth as witnessed by a series of inactive channels seen on the bathymetric data (Fig. 9A; Fabbri *et al.*, 2021), preventing the Aare inflow from fluctuating naturally across the entire valley.

This river correction thus resulted in the present-day location of the Aare River mouth (Fig. 9A). As MT4 is dated between 1822 and 1881 CE (Figs 8C, 8D and 9B), and thus coincides with the onset of these modifications. The authors believe that the modification of the Aare River's course, resulting in a concentrated input of sediment particles at the river mouth, caused a significant and sustainable impact by radically affecting the sedimentation of the Aare Delta. Whereas the river mouth now charges the adjacent slope more rapidly, the remainder of the delta front became sediment starved, increasing the contrast in delta progradation between the mouthing slope area and the abandoned other lateral areas (Silva *et al.*, 2019). Thus, it is suggested herein that the shorter recurrence interval (±50 year) of megaturbidites in the last *ca* 200 years (compared to the former ±230 year recurrence in the last 900 years) is mainly

caused by the human-induced Aare River modification (Fig. 9B) causing a somehow 'human-induced' autocyclic delta-failure pattern. This autocyclicity highlights the possibility that a future megaturbidite event at the Aare Delta will occur in the next two to three decades, redistribute large sediment volumes, affect the lake's hydrology, and potentially cause a tsunami-like wave of at least half a metre amplitude as it did for MT1 in 1996 CE (Girardclos *et al.*, 2007). However, an earlier release of the next collapse by external triggers such as earthquakes or major floods ahead of its 'human-induced' sediment load-related schedule cannot be excluded (Fig. 9B).

CONCLUSION

The present study has provided novel insights into the occurrence of megaturbidites originating from the Aare Delta in Lake Brienz. These events, with average ages of 1853, 1905, 1942 and 1996 CE, represent with their short recurrence interval of *ca* 50 years and their large volumes of up to 2.3×10^6 m^3 unprecedented phenomena over – at least – the past 500 years. The origin of these megaturbidites can be attributed to the focused sediment accumulation at the front of the channelized river inflow in the proximal delta region, caused by the modification of the Aare River through its straightening and channelization during the late 19th century. The *ca* 50 year recurrence interval suggests a human-initiated autocyclic behaviour and the possibility of a future megaturbidite event happening over the next two to three decades. Such events must be taken into account in the natural hazard and risk management of Lake Brienz, especially considering that a tsunami-like wave of at least 0.5 m amplitude was generated in 1996 CE during the last megaturbidite event. Overall, this study highlights the complex dynamics of delta sedimentation in the Anthropocene and the importance of considering human activities (for example, the significant impact of river regulations) and natural triggers in assessing the risks associated with future megaturbidite events and potential tsunamis. This information is essential for implementing effective measures to protect vulnerable communities in delta areas and along coastlines, whether in lakes or marine environments.

ACKNOWLEDGEMENTS

We thank Robert Hofmann, Urs Gerber and Marcel Mettler for technical assistance and Hsin-Chi Lan for SEM analyses. Many thanks to Raphael Bühler, Ignacio Canet, Emmanuel Chapron, Gaudenz Deplazes, Miriam Duehnforth, Chris Krugh, Cecile Matter, Laurie Mauclaire, Nele Meckler, Andreas Mueller, Matthias Papp, Michael Schnellmann, Michael Strasser, Janez Susnik and Rolf Warthmann for their help on the field. We also particularly thank Christoph Studer (Niederried) for the many talks and emails that provided excellent history expertise on the Lake Brienz region as well as Felix Frey from the Federal Office of Topography (Swisstopo) who shared his expertise on historical maps. We are also very grateful to Anton Vos, science journalist at the University of Geneva, who searched and found the 21 September 1913 corpses' event in numerical archives. This project was supported by the Swiss National Science Foundation (Grant 620-066113). Katrina Kremer is currently supported by the Swiss National Science Foundation (Grant 201610). We would also like to thank the three anonymous reviewers and Katleen Wils who took the time to provide us with constructive and positive feedback.

CONFLICT OF INTEREST

The authors declare no conflict of interest.

DATA AVAILABILITY STATEMENT

The sediment cores are stored at ETH Zürich. Seismic data are available on request from the authors.

REFERENCES

Adams, E.W., **Schlager, W.** and **Anselmetti, F.S.** (2001) Morphology and curvature of delta slopes in Swiss lakes: lessons for the interpretation of clinoforms in seismic data. *Sedimentology*, **48**, 661–679.

Anselmetti, F.S., **Bühler, R.**, **Finger, D.**, **Girardclos, S.**, **Lancini, A.**, **Rellstab, C.** and **Sturm, M.** (2007a) Effects of Alpine hydropower dams on particle transport and lacustrine sedimentation. *Aquat. Sci.*, **69**, 179–198.

Anselmetti, F.S., **Hodell, D.A.**, **Ariztegui, D.**, **Brenner, M.** and **Rosenmeier, M.F.** (2007b) Quantification of soil erosion rates related to ancient Maya deforestation. *Geology*, **35**, 915–918.

Arnaud, F., **Poulenard, J.**, **Giguet-Covex, C.**, **Wilhelm, B.**, **Révillon, S.**, **Jenny, J.-P.**, **Revel, M.**, **Enters, D.**, **Bajard, M.**, **Fouinat, L.**, **Doyen, E.**, **Simonneau, A.**, **Pignol, C.**, **Chapron, E.**, **Vannière, B.** and **Sabatier, P.** (2016) Erosion under climate and human pressures: an alpine lake sediment perspective. *Quatern. Sci. Rev.*, **152**, 1–18.

Assier-Rzadkieaicz, S., **Heinrich, P.**, **Sabatier, P.C.**, **Savoye, B.** and **Bourillet, J.F.** (2000) Numerical modelling of a landslide-generated Tsunami: the 1979 nice event. *Pure Appl. Geophys.*, **157**, 1707–1727.

Billi, P. and **Caparrini, F.** (2006) Estimating land cover effects on evapotranspiration with remote sensing: a case study in Ethiopian Rift Valley. *Hydrol. Sci. J.*, **51**, 655–670.

Blaauw, M. and **Christen, J.A.** (2011) Flexible paleoclimate age-depth models using an autoregressive gamma process. *Bayesian Anal.*, **6**, 457–474.

Bundesamt für Umwelt BAFU. (2024) Hydrologische Daten und Vorhersagen. https://www.hydrodaten.admin.ch/. Accessed 21 Jun 2024.

Chapron, E., **Van Rensbergen, P.**, **Beck, C.**, **Batist, M.** and **Paillet, A.** (1996) Lacustrine sedimentary records of brutal events in Lake Le Bourget (Northwestern Alps-Southern Jura) [Enregistrements d'événements brutaux dans la sédimentation lacustre du Lac du Bourget (Alpes occidentales-Jura méridional).]. *Quaternaire*, **7**, 155–168.

Chapron, E., **Beck, C.**, **Pourchet, M.** and **Deconinck, J.-F.** (1999) 1822 earthquake-triggered homogenite in Lake Le Bourget (NW Alps). *Terra Nova*, **11**, 86–92.

Clare, M.A., **Hughes Clarke, J.E.**, **Talling, P.J.**, **Cartigny, M.J.B.** and **Pratomo, D.G.** (2016) Preconditioning and triggering of offshore slope failures and turbidity currents revealed by most detailed monitoring yet at a fjord-head delta. *Earth Planet. Sci. Lett.*, **450**, 208–220.

Coleman, J. and **Prior, D.** (1988) Mass wasting on continental margins. *Annu. Rev. Earth Planet. Sci.*, **16**, 101–119.

Devenish, N. (2015) Gefährlicher Badeplausch. Jungfrau Zeitung. www.jungfrauzeitung.ch. Günter, 2006. Accessed 9 Oct 2023.

Fabbri, S.C., **Buechi, M.W.**, **Horstmeyer, H.**, **Hilbe, M.**, **Hübscher, C.**, **Schmelzbach, C.**, **Weiss, B.** and **Anselmetti, F.S.** (2018) A subaquatic moraine complex in overdeepened Lake Thun (Switzerland) unravelling the deglaciation history of the Aare Glacier. *Quatern. Sci. Rev.*, **187**, 62–79.

Fabbri, S.C., **Haas, I.**, **Kremer, K.**, **Motta, D.**, **Girardclos, S.** and **Anselmetti, F.S.** (2021) Subaqueous geomorphology and delta dynamics of Lake Brienz (Switzerland): implications for the sediment budget in the alpine realm. *Swiss J. Geosci.*, **114**, 1–17.

Fäh, D., **Giardini, D.**, **Kästli, P.**, **Deichmann, N.**, **Gisler, M.**, **Schwarz-Zanetti, G.**, **Alvarez-Rubio, S.**, **Sellami, S.**, **Edwards, B.**, **Allmann, B.**, **Bethmann, F.**, **Woessner, J.**, **Gassner-Stamm, G.**, **Fritsche, S.** and **Eberhard, D.A.J.** (2011) ECOS-09 earthquake catalogue of Switzerland release 2011 report and database. Public catalogue, 17. 4. 2011. Swiss Seismological Service ETH Zurich.

Finger, D., **Schmid, M.** and **Wueest, A.** (2006) Effects of upstream hydropower operation on riverine particle transport and turbidity in downstream lakes. *Water Resour. Res.*, **42**, W08429. https://doi.org/10.1029/2005WR004751.

Geiser, K. (1914) *Brienzersee und Thunersee: Historisches und Rechtliches über den Abfluss*. Buchdr, Rösch & Schatzmann. 174 pp.

Girardclos, S., **Schmidt, O.T.**, **Sturm, M.**, **Ariztegui, D.**, **Pugin, A.** and **Anselmetti, F.S.** (2007) The 1996 AD delta collapse and large turbidite in Lake Brienz. *Mar. Geol.*, **241**, 137–154.

Günter, A.-M. (2006) Kinderstube für Brienzersee-Hechte. Jungfrau Zeitung. www.jungfrauzeitung.ch. https://www.jungfrauzeitung.ch/artikel/62788/. Accessed 9 Oct 2023.

Haughton, P., **Davis, C.**, **McCaffrey, W.** and **Barker, S.** (2009) Hybrid sediment gravity flow deposits–classification, origin and significance. *Mar. Petrol. Geol.*, **26**, 1900–1918.

Hein, C.J., **Fallon, A.R.**, **Rosen, P.**, **Hoagland, P.**, **Georgiou, I.Y.**, **FitzGerald, D.M.**, **Morris, M.**, **Baker, S.**, **Marino, G.B.** and **Fitzsimons, G.** (2019) Shoreline dynamics along a developed river mouth Barrier Island: multi-decadal cycles of erosion and event-driven mitigation. *Front. Earth Sci.*, **7**, 103. https://doi.org/10.3389/feart.2019.00103.

Hilbe, M. and **Anselmetti, F.S.** (2014) Signatures of slope failures and river-delta collapses in a perialpine lake (Lake Lucerne, Switzerland). *Sedimentology*, **61**, 1883–1907.

Kelts, K., **Briegel, U.**, **Ghilardi, K.** and **Hsu, K.** (1986) The limnogeology-ETH coring system. *Schweiz. Z. Hydrol.*, **48**, 104–115.

Kempf, P. and **Moernaut, J.** (2021) Age uncertainty in recurrence analysis of paleoseismic records. *J. Geophys. Res. Solid Earth*, **126**, e2021JB021996.

Kempf, P., **Moernaut, J.** and **Batist, M.D.** (2018) Bimodal recurrence pattern of Tsunamis in South-Central Chile: a statistical exploration of paleotsunami data. *Seismol. Res. Lett.*, **90**, 194–202.

Kesel, R.H. (2003) Human modifications to the sediment regime of the Lower Mississippi River flood plain. *Geomorphology*, **56**, 325–334.

Kremer, K., **Simpson, G.** and **Girardclos, S.** (2012) Giant Lake Geneva tsunami in AD 563. *Nat. Geosci.*, **5**, 756–757.

Kurz, C. and **Lerch, C.** (1979) Geschichte der Landschaft Hasli. *Brügger*, 694 pp.

Lane, S.N., **Bakker, M.**, **Costa, A.**, **Girardclos, S.**, **Loizeau, J.-L.**, **Molnar, P.**, **Silva, T.**, **Stutenbecker, L.** and **Schlunegger, F.** (2019) Making stratigraphy in the Anthropocene: climate change impacts and economic conditions controlling the supply of sediment to Lake Geneva. *Sci. Rep.*, **9**, 8904.

Leithold, E.L., **Wegmann, K.W.**, **Bohnenstiehl, D.R.**, **Joyner, C.N.** and **Pollen, A.F.** (2019) Repeated megaturbidite deposition in Lake Crescent, Washington, USA, triggered by Holocene ruptures of the Lake Creek-Boundary Creek fault system. *GSA Bull.*, **131**, 2039–2055.

Masson-Delmotte, V., **Schulz, M.**, **Abe-Ouchi, A.**, **Beer, J.**, **Ganopolski, A.**, **González Rouco, J.F.**, **Jansen, E.**, **Lambeck, K.**, **Luterbacher, J.**, **Naish, T.**, **Osborn, T.**, **Otto-Bliesner, B.**, **Quinn, T.**, **Ramesh, R.**, **Rojas, M.**, **Shao, X.** and **Timmermann, A.** (2013) Information from paleoclimate archives. In: *Climate Change 2013: The Physical Science Basis. Contribution of Working Group I to the Fifth Assessment Report of the Intergovernmental Panel on Climate Change* (Eds Stocker, T.F., Qin, D., Plattner, G.-K., Tignor, M., Allen, S.K., Boschung, J., Nauels, A., Xia, Y., Bex, V. and Midgley, P.M.). Cambridge University Press, Cambridge, UK.

Matter, A., **Dessolin, D.**, **Sturm, M.** and **Süsstrunk, A.** (1973) Reflexionsseismische Untersuchungen im Brienzersee. *Eclogae Geol. Helv.*, **66**, 71–82.

Mazure, T., **Saulnier, G.-M.**, **Giguet-Covex, C.**, **Sabatier, P.**, **Bajard, M.**, **Chanudet, V.**, **Arnaud, F.** and **Jenny, J.-P.** (2024) Half of the soil erosion in the Alps during the Holocene is explained by transient erosion crises as a

consequence of rapid human land clearing. *The Holocene*. https://doi.org/10.1177/09596836241254485

Mirani, A. (1764) Aare, Meiringen - Brienzersee: "Plan topographique du cours de l'Aar dans la plaine ou vallée d'Oberhasli jusques au lac de Brientz"; mit Kanalprojekt. 1:5′000. Inventaire en ligne des Archives de l'Etat de Berne. https://www.query.sta.be.ch/detail.aspx?ID=364978. Accessed 25 Oct 2023.

Moernaut, J., **Daele, M.V.**, **Heirman, K.**, **Fontijn, K.**, **Strasser, M.**, **Pino, M.**, **Urrutia, R.** and **De Batist, M.** (2014) Lacustrine turbidites as a tool for quantitative earthquake reconstruction: new evidence for a variable rupture mode in south central Chile. *J. Geophys. Res. Solid Earth*, **119**, 1607–1633.

Nigg, V., **Wohlwend, S.**, **Hilbe, M.**, **Bellwald, B.**, **Fabbri, S.C.**, **de Souza, G.F.**, **Donau, F.**, **Grischott, R.**, **Strasser, M.** and **Anselmetti, F.S.** (2021) A tsunamigenic delta collapse and its associated tsunami deposits in and around Lake Sils, Switzerland. *Nat. Hazards*, **107**, 1069–1103.

Niklaus, M. (1968) Wildbäche und Lawinen am rechten Brienzerseeufer. Jahrbuch vom Thuner- und Brienzersee, Jahr, 1968, 23–36.

Nydegger, P. (1967) Untersuchungen über Feinststofftransport in Flüssen und Seen, über Entstehung von Trübungshorizonten und zuflussbedingten Strömungen im Brienzersee und einigen Vergleichsseen.

Nydegger, P. (1976) Strömungen in Seen. *Untersuchungen in situ und an nachgebildeten Modellseen. Beitr. Geol. Schweiz Klein. Mitt*, **66**, 141–177.

Oberländer, T. (1913) Oberländer Tagblatt. In: 1909-: [Thun] : Stüssy & Muntwyler, [1909-1961] <1938>−1961: Thun : Druck- und Verlagsanstalt Adolf Schaer. https://www.e-newspaperarchives.ch/?a=d&d=BUR19130927-01.2.9. Accessed 22 Jan 2024.

Oberländer, T. (1942) Oberländer Tagblatt. In: 1909-: [Thun] : Stüssy & Muntwyler, [1909-1961] <1938>−1961: Thun : Druck- und Verlagsanstalt Adolf Schaer. https://www.e-newspaperarchives.ch/?a=d&d=OTB19420921-01. Accessed 19 May 2023.

Petroni, B. (2010) Badegäste tummeln sich auf verbotener Sandbank. Berner Zeitung. Berner Zeitung. https://www.bernerzeitung.ch/badegaeste-tummeln-sich-auf-verbotener-sandbank-119996496297. Accessed 9 Oct 2023.

Pfister, C. (2009) Die, Katastrophenlücke "des 20". Jahrhunderts und der Verlust traditionalen Risikobewusstseins. *GAIA-Ecol. Perspect Sci. Soc.*, **18**, 239–246.

Pfister, C., **Luterbacher, J.** and **Wanner, H.** (1999) Wetternachhersage: 500 Jahre Klimavariationen und Naturkatastrophen (1496–1995). *P. Haupt*.

Praet, N., **Moernaut, J.**, **Van Daele, M.**, **Boes, E.**, **Haeussler, P.J.**, **Strupler, M.**, **Schmidt, S.**, **Loso, M.G.** and **De Batist, M.** (2017) Paleoseismic potential of sublacustrine landslide records in a high-seismicity setting (south-central Alaska). *Mar. Geol.*, **384**, 103–119.

Prior, D., **Yang, Z.-S.**, **Bornhold, B.**, **Keller, G.**, **Lu, N.**, **Wiseman, W.**, **Wright, L.** and **Zhang, J.** (1986) Active slope failure, sediment collapse, and silt flows on the modern subaqueous Huanghe (Yellow River) delta. *Geo-Mar. Lett.*, **6**, 85–95.

Reimer, P.J., **Austin, W.E.**, **Bard, E.**, **Bayliss, A.**, **Blackwell, P.G.**, **Ramsey, C.B.**, **Butzin, M.**, **Cheng, H.**, **Edwards, R.L.**, **Friedrich, M.**, **Grootes, P.M.**, **Guilderson, T.P.**, **Hajdas, I.**, **Heaton, T.J.**, **Hogg, A.G.**, **Hughen, K.A.**, **Kromer, B.**, **Manning, S.W.**, **Muscheler, R.**, **Palmer, J.G.**, **Pearson, C.**, **van der Plicht, J.**, **Reimer, R.W.**, **Richards, D.A.**, **Scott, E.M.**, **Southon, J.R.**, **Turney, C.S.**, **Wacker, L.**, **Adolphi, F.**, **Büntgen, U.**, **Capano, M.**, **Fahrni, S.M.**, **Fogtmann-Schulz, A.**, **Friedrich, R.**, **Köhler, P.**, **Kudsk, S.**, **Miyake, F.**, **Olsen, J.**, **Reinig, F.**, **Sakamoto, M.**, **Sookdeo, A.** and **Talamo, S.** (2020) The IntCal20 Northern Hemisphere radiocarbon age calibration curve (0–55 cal kBP). *Radiocarbon*, **62**, 1–33.

Röthlisberger, G. (1991) Chronik der Unwetterschäden in der Schweiz. In: *Berichte der Eidgenössischen Forschungsanstalt für Wald, Schnee und Landschaft: Vol. 330*, p. 122. Eidgenössische Forschungsanstalt für Wald, Schnee und Landschaft, Birmensdorf.

Röthlisberger, G. (1998) Unwetterschäden in der Schweiz. Berichte der Eidgenössischen Forschungsanstalt für Wald, Schnee und Landschaft. *WSL*, Birmensdorf.

Sabatier, P., **Moernaut, J.**, **Bertrand, S.**, **Van Daele, M.**, **Kremer, K.**, **Chaumillon, E.** and **Arnaud, F.** (2022) A review of event deposits in lake sediments. *Quaternary*, **5**, 34.

Schulte, L., **Veit, H.**, **Burjachs, F.** and **Julià, R.** (2009) Lütschine fan delta response to climate variability and land use in the Bernese Alps during the last 2400 years. *Geomorphology*, **108**, 107–121.

Schulte, L., **Peña, J.C.**, **Carvalho, F.**, **Schmidt, T.**, **Julià, R.**, **Llorca, J.** and **Veit, H.** (2015) A 2600-year history of floods in the Bernese Alps, Switzerland: frequencies, mechanisms and climate forcing. *Hydrol. Earth Syst. Sci.*, **19**, 3047–3072.

Shynkarenko, A., **Cauzzi, C.**, **Kremer, K.**, **Bergamo, P.**, **Lontsi, A.**, **Janusz, P.** and **Fäh, D.** (2023) On the seismic response and earthquake-triggered failures of subaqueous slopes in Swiss lakes. *Geophys. J. Int.*, 235, 566–588.

Silva, T.A., **Girardclos, S.**, **Stutenbecker, L.**, **Bakker, M.**, **Costa, A.**, **Schlunegger, F.**, **Lane, S.N.**, **Molnar, P.** and **Loizeau, J.-L.** (2019) The sediment budget and dynamics of a delta-canyon-lobe system over the Anthropocene timescale: The Rhone River delta, Lake Geneva (Switzerland/France). *Sedimentology*, **66**, 838–858.

Strupler, M., **Hilbe, M.**, **Kremer, K.**, **Danciu, L.**, **Anselmetti, F.S.**, **Strasser, M.** and **Wiemer, S.** (2018) Subaqueous landslide-triggered tsunami hazard for Lake Zurich, Switzerland. *Swiss J. Geosci.*, **111**, 353–371.

Sturm, M. (1976) Die Oberflächensedimente Des Brienzersees. *Eclogae Geologicae Helvetiae*, **69**, 111–123.

Sturm, M. and **Matter, A.** (1978) Turbidites and varves in Lake Brienz (Switzerland): deposition of clastic detritus by density currents. In: *Modern and Ancient Lake Sediments* (Eds Matter, A. and Tucker, M.E.), pp. 147–168. Special Publications International Association of Sedimentologists, Oxford.

Talling, P., **Amy, L.**, **Wynn, R.**, **Peakall, J.** and **Robinson, M.** (2004) Beds comprising debrite sandwiched within co-genetic turbidite: origin and widespread occurrence in distal depositional environments. *Sedimentology*, **51**, 163–194.

Talling, P.J., **Masson, D.G.**, **Sumner, E.J.** and **Malgesini, G.** (2012) Subaqueous sediment density flows: Depositional processes and deposit types. *Sedimentology*, **59**, 1937–2003.

Terrinha, P., **Duarte, H.**, **Brito, P.**, **Noiva, J.**, **Ribeiro, C.**, **Omira, R.**, **Baptista, M.A.**, **Miranda, M.**, **Magalhães, V.** and **Roque, C.** (2019) The Tagus River delta landslide, off Lisbon, Portugal. Implications for Marine geo-hazards. *Mar. Geol.*, **416**, 105983.

Van Daele, M., **Moernaut, J.**, **Doom, L.**, **Boes, E.**, **Fontijn, K.**, **Heirman, K.**, **Vandoorne, W.**, **Hebbeln, D.**, **Pino, M.**, **Urrutia, R.**, **Brümmer, R.** and **De Batist, M.** (2015) A comparison of the sedimentary records of the 1960 and

2010 great Chilean earthquakes in 17 lakes: implications for quantitative lacustrine palaeoseismology. *Sedimentology*, **62**, 1466–1496.

Vanneste, K., **Wils, K.** and **Van Daele, M.** (2018) Probabilistic evaluation of fault sources based on paleoseismic evidence from mass-transport deposits: the example of Aysén Fjord, Chile. *J. Geophys. Res. Solid Earth*, **123**, 9842–9865.

Vischer, D.L. (2003) Histoire de la protection contre les crues en Suisse. *Rapports de l'OFEG, Série Eaux*, **5**, 208.

Vörösmarty, C.J., **Sharma, K.P.**, **Fekete, B.M.**, **Copeland, A.H.**, **Holden, J.**, **Marble, J.** and **Lough, J.A.** (1997) The storage and aging of continental runoff in large reservoir systems of the world.

Vörösmarty, C.J., **Meybeck, M.**, **Fekete, B.**, **Sharma, K.**, **Green, P.** and **Syvitski, J.P.** (2003) Anthropogenic sediment retention: major global impact from registered river impoundments. *Glob. Planet. Change*, **39**, 169–190.

Williams, R.T., **Davis, J.R.** and **Goodwin, L.B.** (2019) Do large earthquakes occur at regular intervals through time? A perspective from the geologic record. *Geophys. Res. Lett.*, **46**, 8074–8081.

World Health Organization (1982) *Manual on Environmental Management for Mosquito Control, with Special Emphasis on Malaria Vectors*. World Health Organization, Geneva (Switzerland). https://iris.who.int/handle/10665/37329.

Yuan, W., **Yin, D.**, **Finlayson, B.** and **Chen, Z.** (2012) Assessing the potential for change in the middle Yangtze River channel following impoundment of the Three Gorges Dam. *Geomorphology*, **147**, 27–34.

Manuscript received 25 October 2023; revision accepted 17 July 2024

Supporting Information

Additional information may be found in the online version of this article:

Figure S1. Topographic map of the Aare River course from Oberhasli to Lake Brienz (1764).

Figure S2. Photographs and core-to-core visual correlation (short core BR03-20, core section BR05-5-KK, core section BR05-5-11, short core BR98-16 and short core BR03-10) to infer ages of the two most recent megaturbidites MT1 and MT2 and using radionuclides ages from Anselmetti *et al.* (2007) and Girardclos *et al.* (2007).

Figure S3. Map of the historical earthquakes from the ECOS catalogue (http://ecos09.seismo.ethz.ch), from 1800 CE to 2020 CE, with a radial width of 200 km around Lake Brienz (white transparent circle).

Figure S4. A 3.5 kHz longitudinal seismic section from 2018 is displayed, with the raw data on the top panel and the interpreted profile at the bottom panel.

Figure S5. Plot representing the conditional probability of a megaturbidite event every five years from the last MT1 event (associated to delta collapse) in 1996 to 2124 CE (100 years after this study), using a normal distribution and the recurrence between each event (47.7 ± 13.08 years).

Table S1. List of historical flood events (13th century to present) potentially affecting Lake Brienz catchment area from historical data in Switzerland (Niklaus, 1968; Kurz & Lerch, 1979; Röthlisberger, 1991, 1998; Pfister et al., 1999; Vischer, 2003).

Table S2. List of historical earthquakes from the ECOS catalogue (http://ecos09.seismo.ethz.ch), from 1800 CE to 2020 CE, with a radial width of 200 km around Lake Brienz and with local intensities greater than II at the Aare Delta location (46.74N; 8.04E).

Table S3. Sedimentation rates for the background sedimentation (Lithotype 1), the turbidites (Lithotype 2a) and the whole sediment sequence, calculated for the inter-megaturbidite phases (Fig. 7B).